J|A|C|S
ARTICLES
Published on Web 07/20/2006

Ethyne-Bridged (Porphinato)Zinc(II)−(Porphinato)Iron(III) Complexes: Phenomenological Dependence of Excited-State Dynamics upon (Porphinato)Iron Electronic Structure

Timothy V. Duncan, Sophia P. Wu, and Michael J. Therien*

Contribution from the Department of Chemistry, University of Pennsylvania, Philadelphia, Pennsylvania 19104-6323

Received February 28, 2006; E-mail: therien@sas.upenn.edu

Abstract: We report the synthesis, spectroscopy, potentiometric properties, and excited-state dynamical studies of 5-[(10,20-di-((4-ethyl ester)methylene-oxy)phenyl)porphinato]zinc(II)−[5′-[(10′,20′- di-((4-ethyl ester)methylene-oxy)phenyl)porphinato]iron(III)-chloride]ethyne (**PZn**−**PFe-Cl**), along with a series of related supermolecules (**[PZn**−**PFe-(L)$_{1,2}$]**$^+$ species) that possess a range of metal axial ligation environments (L = pyridine, 4-cyanopyridine, 2,4,6-trimethylpyridine (collidine), and 2,6-dimethylpyridine (2,6-lutidine)). Relevant monomeric [(porphinato)iron-(ligand)$_{1,2}$]$^+$ (**[PFe(L)$_{1,2}$]**$^+$) benchmarks have also been synthesized and fully characterized. Ultrafast pump−probe transient absorption spectroscopic experiments that interrogate the initially prepared electronically excited states of **[PFe(L)$_{1,2}$]**$^+$ species bearing nonhindered axial ligands demonstrated subpicosecond-to-picosecond relaxation dynamics to the ground electronic state. Comparative pump−probe transient absorption experiments that interrogate the initially prepared excited states of **PZn**−**PFe-Cl**, **[PZn**−**PFe-(py)$_2$]**$^+$, **[PZn**−**PFe-(4-CN-py)$_2$]**$^+$, **[PZn**−**PFe-(collidine)]**$^+$, and **[PZn**−**PFe-(2,6-lutidine)]**$^+$ demonstrate that the spectra of all these species are dominated by a broad, intense NIR $S_1 \rightarrow S_n$ transient absorption manifold. While **PZn**−**PFe-Cl***, **[PZn**−**PFe-(py)$_2$]**$^+$*, and **[PZn**−**PFe-(4-CN-py)$_2$]**$^+$* evince subpicosecond and picosecond time-scale relaxation of their respective initially prepared electronically excited states to the ground state, the excited-state dynamics observed for **[PZn**−**PFe-(2,6-lutidine)]**$^+$* and **[PZn**−**PFe-(collidine)]**$^+$* show fast relaxation to a [PZn$^+$−PFe(II)] charge-separated state having a lifetime of nearly 1 ns. Potentiometric data indicate that while ΔG_{CS} for **[PZn**−**PFe-(L)$_{1,2}$]**$^+$* species is strongly influenced by the PFe$^+$ ligation state [ligand (ΔG_{CS}): 4-cyanopyridine (−0.79 eV) < pyridine (−1.04 eV) < collidine (−1.35 eV) < chloride (−1.40 eV); solvent = CH_2Cl_2], the pump−probe transient absorption dynamical data demonstrate that the nature of the dominant excited-state decay pathway is not correlated with the thermodynamic driving force for photoinduced charge separation, but depends on the ferric ion ligation mode. These data indicate that sterically bulky axial ligands that drive a pentacoordinate PFe center and a weak metal axial ligand interaction serve to sufficiently suppress the normally large magnitude nonradiative decay rate constants characteristic of (porphinato)iron(III) complexes, and thus make electron transfer a competitive excited-state deactivation pathway.

Introduction

Understanding charge- and excitation-migration reactions in multipigment assemblies is essential for biomimetic modeling of energy transduction and for the eventual design and development of supramolecular systems relevant to artificial photosynthesis,[1−19] materials chemistry,[20−27] and optoelectronics[28−42] that exploit biologically inspired chromophoric building blocks. Strong interpigment coupling is a common feature of such functional materials; as such, considerable effort has focused

(1) Van Patten, P. G.; Shreve, A. P.; Lindsey, J. S.; Donohoe, R. J. *J. Phys. Chem. B* **1998**, *102*, 4209−4216.
(2) Sessler, J. L.; Johnson, M. R.; Lin, T.-Y.; Creager, S. E. *J. Am. Chem. Soc.* **1988**, *110*, 3659−3661.
(3) Gust, D.; Moore, T. A. *Science* **1989**, *244*, 35−41.
(4) Sessler, J. L.; Johnson, M. R.; Creager, S. E.; Fettinger, J. C.; Ibers, J. A. *J. Am. Chem. Soc.* **1990**, *112*, 9310−9329.
(5) Osuka, A.; Nagata, T.; Maruyama, K.; Mataga, N.; Asahi, T.; Yamazaki, I.; Nishimura, Y. *Chem. Phys. Lett.* **1991**, *185*, 88−94.
(6) Gust, D.; Moore, T. A.; Moore, A. L.; Gao, F.; Luttrull, D.; DeGraziano, J. M.; Ma, X. C.; Makings, L. R.; Lee, S.-J.; Trier, T. T.; Bittersmann, E.; Seely, G. R.; Woodward, S.; Bensasson, R. V.; Rougee, M.; De Schryver, F. C.; Van der Auweraer, M. *J. Am. Chem. Soc.* **1991**, *113*, 3638−3649.
(7) Wasielewski, M. R. *Chem. Rev.* **1992**, *92*, 435−461.
(8) Gust, D.; Moore, T. A.; Moore, A. L.; Leggett, L.; Lin, S.; DeGraziano, J. M.; Hermant, R. M.; Nicodem, D.; Craig, P.; Seely, G. R.; Nieman, R. A. *J. Phys. Chem.* **1993**, *97*, 7926−7931.
(9) Osuka, A.; Nakajima, S.; Maruyama, K.; Mataga, N.; Asahi, T.; Yamazaki, I.; Nishimura, Y.; Ohno, T.; Nozaki, K. *J. Am. Chem. Soc.* **1993**, *115*, 4577−4589.
(10) Sessler, J. L.; Capuano, V. L.; Harriman, A. *J. Am. Chem. Soc.* **1993**, *115*, 4618−4628.
(11) Osuka, A.; Marumo, S.; Taniguchi, S.; Okada, T.; Mataga, N. *Chem. Phys. Lett.* **1994**, *230*, 144−148.
(12) Lin, V. S.-Y.; DiMagno, S. G.; Therien, M. J. *Science* **1994**, *264*, 1105−1111.
(13) Lin, V. S.-Y.; Therien, M. J. *Chem. Eur. J.* **1995**, *1*, 645−651.
(14) Hsiao, J.-S.; Krueger, B. P.; Wagner, R. W.; Johnson, T. E.; Delaney, J. K.; Mauzerall, D. C.; Fleming, G. R.; Lindsey, J. S.; Bocian, D. F.; Donohoe, R. J. *J. Am. Chem. Soc.* **1996**, *118*, 11181−11193.
(15) Steinberg-Yfrach, G.; Liddell, P. A.; Hung, S.-C.; Moore, A. L.; Gust, D.; Moore, T. A. *Nature* **1997**, *385*, 239−241.
(16) Hu, Y.-Z.; Tsukiji, S.; Shinkai, S.; Oishi, S.; Hamachi, I. *J. Am. Chem. Soc.* **2000**, *122*, 241−253.
(17) Choi, M.-S.; Yamazaki, T.; Yamazaki, I.; Aida, T. *Angew. Chem., Int. Ed.* **2004**, *43*, 150−158.
(18) Imahori, H. *J. Phys. Chem. B* **2004**, *108*, 6130−6143.
(19) D'Souza, F.; Smith, P. M.; Zandler, M. E.; McCarty, A. L.; Itou, M.; Araki, Y.; Ito, O. *J. Am. Chem. Soc.* **2004**, *126*, 7898−7907.

on interrogating the photophysics of covalently linked assemblies of porphyrins and related polypyrrolic macrocycles where chromophore−chromophore electronic interactions give rise to extensively delocalized electronically excited states.[12,13,35,36,43−62]

While considerable progress has been made with respect to understanding the fundamental excited-state dynamics of strongly coupled porphyrinoid compounds,[35,49,62] little is known regarding the corresponding excited-state delocalization-, electron-, and energy-transfer dynamics of related systems that possess open *d*-electron shells. Here, we report the synthesis, spectroscopy, and potentiometric and excited-state dynamical studies of 5-[(10,20-di-(((4-ethyl ester)methylene-oxy)phenyl)porphinato)-zinc(II)]−[5′-[(10′,20′- di-(((4-ethyl ester)methylene-oxy)phenyl)porphinato)iron(III)-chloride]ethyne (**PZn−PFe-Cl**), along with a series of related compounds that possess a range of metal axial ligation environments. Application of femtosecond (fs) transient absorption spectroscopy shows that the evolution of the initially prepared electronically excited states of these supermolecular, *meso*-to-*meso* ethyne-bridged PZn−PFe(III) compounds is governed by the axial ligation state of the (porphinato)iron center.

Experimental Section

Materials. All manipulations were carried out under nitrogen previously passed through an O_2 scrubbing tower (Schweitzerhall R3-11 catalyst) and a drying tower (Linde 3 Å molecular sieves) unless otherwise stated. Air-sensitive solids were handled in a Braun 150-M glovebox. Standard Schlenk techniques were employed to manipulate air-sensitive solutions. Methylene chloride (CH_2Cl_2) and tetrahydrofuran (THF) were distilled from CaH_2 and K/4-benzoylbiphenyl, respectively, under N_2. Nitrogenous ligands were purchased from Aldrich and used as received. Acetone was dried over K_2CO_3 overnight and filtered prior to use. Absolute ethanol (Fisher Scientific), as well as NMR solvents, was used as received. $ZnCl_2$ was dried by heating under vacuum and stored under N_2. The catalysts, tetrakis(triphenylphosphine)palladium ($Pd(PPh_3)_4$), tris(dibenzylideneacetone)dipalladium (Pd_2dba_3), and triphenylarsine ($AsPh_3$) were purchased from Strem Chemicals.

Chemical shifts for ^1H NMR spectra are reported relative to residual protium in the deuterated solvents ($CDCl_3$, $\delta = 7.24$ ppm; pyridine-d_5, $\delta = 7.19$ ppm, C_6D_6, $\delta = 7.15$ ppm). The number of attached protons is found in parentheses following the chemical shift value. Flash column chromatography was performed on the benchtop, using silica gel (230−400 mesh) obtained from EM Science. High-resolution electrospray mass spectra were acquired at the Mass Spectrometry Center at the University of Pennsylvania. MALDI-TOF mass spectroscopic data were obtained with a Perspective Voyager DE instrument in the Laboratory of Dr. Virgil Percec (Department of Chemistry, University of Pennsylvania). Samples were prepared as micromolar solutions in THF, and dithranol (Aldrich) was utilized as the matrix. Fast atom bombardment (FAB) mass spectrometry analyses were performed at the Mass Spectrometry Center at Drexel University.

Instrumentation. Electronic spectra were recorded on an OLIS UV/vis/near-IR spectrophotometry system that is based on the optics of a Cary 14 spectrophotometer. NMR spectra were recorded on either 250 MHz AC-250 or 360 MHz DMX-360 Brüker spectrometers. Cyclic voltammetric experiments were performed with an EG&G Princeton Applied Research model 273A potentiostat/galvanostat. A single-compartment electrochemical cell with glassy carbon working electrode was used. Steady-state fluorescence emission spectra were recorded on a SPEX Fluorolog 3 spectrometer that utilized a T-channel configuration and PMT/InGaAs/Extended-InGaAs detectors; these spectra were corrected using the spectral output of a calibrated light source supplied by the National Bureau of Standards.

Magnetic Susceptibility Measurements and Ferric Spin State Determination. The spin states of iron(III) in the monomeric complexes were determined by the Evans method.[63] These measurements were carried out in 5-mm diameter NMR tubes that featured 1-mm diameter

(20) Kampas, F. J.; Yamashita, K.; Fajer, J. *Nature* **1980**, *284*, 40−42.
(21) Gregg, B. A.; Fox, M. A.; Bard, A. J. *J. Phys. Chem.* **1990**, *94*, 1586−1598.
(22) Miller, J. S.; Epstein, A. J. *Angew. Chem., Int. Ed. Engl.* **1994**, *33*, 385−415.
(23) Arnold, D. P.; Manno, D.; Micocci, G.; Serra, A.; Tepore, A.; Valli, L. *Langmuir* **1997**, *13*, 5951−5956.
(24) Ikkala, O.; ten Brinke, G. *Science* **2002**, *295*, 2407−2409.
(25) Ostrowski, J. C.; Susumu, K.; Robinson, M. R.; Therien, M. J.; Bazan, G. *Adv. Mater.* **2003**, *15*, 1296−1300.
(26) Hirata, N.; Lagref, J.-J.; Palomares, E. J.; Durrant, J. R.; Nazeeruddin, M. K.; Gratzel, M.; Di Censo, D. *Chem. Eur. J.* **2004**, *10*, 595−602.
(27) Leclere, P.; Surin, M.; Jonkheijm, P.; Henze, O.; Schenning, A. P. H. J.; Biscarini, F.; Grimsdale, A. C.; Feast, W. J.; Meijer, E. W.; Mullen, K.; Bredas, J. L.; Lazzaroni, R. *Eur. Polym. J.* **2004**, *40*, 885−892.
(28) O'Neil, M. P.; Niemczyk, M. P.; Svec, W. A.; Gosztola, D.; Gaines, G. L., III ; Wasielewski, M. R. *Science* **1992**, *257*, 63−65.
(29) Anderson, H. L.; Martin, S. J.; Bradley, D. D. C. *Angew. Chem., Int. Ed. Engl.* **1994**, *33*, 655−657.
(30) DiMagno, S. G.; Lin, V. S.-Y.; Therien, M. J. *J. Am. Chem. Soc.* **1993**, *115*, 2513−2515.
(31) Debreczeny, M. P.; Svec, W. A.; Wasielewski, M. R. *Science* **1996**, *274*, 584−587.
(32) Wagner, R. W.; Lindsey, J. S.; Seth, J.; Palaniappan, V.; Bocian, D. F. *J. Am. Chem. Soc.* **1996**, *118*, 3996−3997.
(33) LeCours, S. M.; Guan, H.-W.; DiMagno, S. G.; Wang, C. H.; Therien, M. J. *J. Am. Chem. Soc.* **1996**, *118*, 1497−1503.
(34) Priyadarshy, S.; Therien, M. J.; Beratan, D. N. *J. Am. Chem. Soc.* **1996**, *118*, 1504−1510.
(35) O'Keefe, G. E.; Denton, G. J.; Harvey, E. J.; Phillips, R. T.; Friend, R. H.; Anderson, H. L. *J. Chem. Phys.* **1996**, *104*, 805−811.
(36) Beljonne, D.; O'Keefe, G. E.; Hamer, P. J.; Friend, R. H.; Anderson, H. L.; Bredas, J. L. *J. Chem. Phys.* **1997**, *106*, 9439−9460.
(37) Karki, L.; Vance, F. W.; Hupp, J. T.; LeCours, S. M.; Therien, M. J. *J. Am. Chem. Soc.* **1998**, *120*, 2606−2611.
(38) Lukas, A. S.; Miller, S. E.; Wasielewski, M. R. *J. Phys. Chem. B* **2000**, *104*, 931−940.
(39) Balzani, V.; Credi, A.; Raymo, F. M.; Stoddart, J. F. *Angew. Chem., Int. Ed.* **2000**, *39*, 3348−3391.
(40) Uyeda, H. T.; Zhao, Y.; Wostyn, K.; Asselberghs, I.; Clays, K.; Persoons, A.; Therien, M. J. *J. Am. Chem. Soc.* **2002**, *124*, 13806−13813.
(41) Kobuke, Y.; Ogawa, K. *Bull. Chem. Soc. Jpn.* **2003**, *76*, 689−708.
(42) O'Neill, M.; Kelly, S. M. *Adv. Mater.* **2003**, *15*, 1135−1146.
(43) Arnold, D. P.; Heath, G. A. *J. Am. Chem. Soc.* **1993**, *115*, 12197−12198.
(44) Anderson, H. L. *Inorg. Chem.* **1994**, *33*, 972−981.
(45) Crossley, M. J.; Govenlock, L. J.; Prashar, J. K. *J. Chem. Soc., Chem. Commun.* **1995**, 2379−2380.
(46) Angiolillo, P. J.; Lin, V. S.-Y.; Vanderkooi, J. M.; Therien, M. J. *J. Am. Chem. Soc.* **1995**, *117*, 12514−12527.
(47) Wytko, J.; Berl, V.; McLaughlin, M.; Tykwinski, R. R.; Schreiber, M.; Diederich, F.; Boudon, C.; Gisselbrecht, J.-P.; Gross, M. *Helv. Chim. Acta* **1998**, *81*, 1964−1977.
(48) Qureshi, F. M.; Martin, S. J.; Long, X.; Bradley, D. D. C.; Henari, F. Z.; Blau, W. J.; Smith, E. C.; Wang, C. H.; Kar, A. K.; Anderson, H. L. *Chem. Phys.* **1998**, *231*, 87−94.
(49) Kumble, R.; Palese, S.; Lin, V. S. Y.; Therien, M. J.; Hochstrasser, R. M. *J. Am. Chem. Soc.* **1998**, *120*, 11489−11498.
(50) Arnold, D. P.; Heath, G. A.; James, D. A. *J. Porphyrins Phthalocyanines* **1999**, *3*, 5−31.
(51) Jiang, B.; Yang, S.-W.; Barbini, D. C.; Jones, W. E. J. *Chem. Commun.* **1998**, 213−214.
(52) Shultz, D. A.; Lee, H.; Kumar, R. K.; Gwaltney, K. P. *J. Org. Chem.* **1999**, *64*, 9124−9136.
(53) Paolesse, R.; Jaquinod, L.; Della Sala, F.; Nurco, D. J.; Prodi, L.; Montalti, M.; Di Natale, C.; D'Amico, A.; Di Carlo, A.; Lugli, P.; Smith, K. M. *J. Am. Chem. Soc.* **2000**, *122*, 11295−11302.
(54) Kuebler, S. M.; Denning, R. G.; Anderson, H. L. *J. Am. Chem. Soc.* **2000**, *122*, 339−347.
(55) Shediac, R.; Gray, M. H. B.; Uyeda, H. T.; Johnson, R. C.; Hupp, J. T.; Angiolillo, P. J.; Therien, M. J. *J. Am. Chem. Soc.* **2000**, *122*, 7017−7033.
(56) Fletcher, J. T.; Therien Michael, J. *J. Am. Chem. Soc.* **2000**, *122*, 12393−12394.
(57) Tsuda, A.; Osuka, A. *Science* **2001**, *293*, 79−82.
(58) Screen, T. E. O.; Thorne, J. R. G.; Denning, R. G.; Bucknall, D. G.; Anderson, H. L. *J. Am. Chem. Soc.* **2002**, *124*, 9712−9713.
(59) Fletcher, J. T.; Therien Michael, J. *J. Am. Chem. Soc.* **2002**, *124*, 4298−4311.
(60) Fletcher, J. T.; Therien, M. J. *Inorg. Chem.* **2002**, *41*, 331−341.
(61) Susumu, K.; Therien, M. J. *J. Am. Chem. Soc.* **2002**, *124*, 8550−8552.
(62) Rubtsov, I., V.; Susumu, K.; Rubtsov, G. I.; Therien, M. J. *J. Am. Chem. Soc.* **2003**, *125*, 2687−2696.
(63) Evans, D. F.; James, T. A. *J. Chem. Soc., Dalton Trans.* **1979**, 723−726.

inner tubes. The inner tube contained solvent, the complex, and a standard, while the outer region contained only solvent and the standard. The magnetic susceptibility per gram, χ_i, was determined by the expression:

$$\chi_i = \frac{-3}{4m\pi}\left(\frac{\nu_0 - \nu_i}{\nu_s}\right) + \chi_0 \quad (1)$$

In this equation, ν_0 and ν_i are the respective chemical shift values, expressed in Hertz, of the standard in the absence (outer tube) and presence (inner tube) of the paramagnetic species; ν_s is the resonance frequency of the spectrometer (500 MHz); m is the concentration of paramagnetic species in the inner tube expressed in grams per cubic centimeter; and χ_0 is the magnetic susceptibility per gram of the standard. The magnetic susceptibility per mole of the paramagnetic species, χ_m, is determined by multiplying χ_i by the molar mass. Finally, the magnetic moment (units of Bohr magneton) can be determined from the molar susceptibility by a formulation of Curie's Law:

$$\mu = 2.84\sqrt{\chi_M T} \quad (2)$$

Here, T is the temperature in K. Since the magnetic moment is also given by

$$\mu = 2\sqrt{S(S+1)} \quad (3)$$

the spin state of the paramagnetic species can easily be estimated from the experimentally determined value.

For these experiments, trimethylorthoformate (1,1,1-trimethoxymethane) was chosen as a standard because of its low molecular weight and its sharp NMR singlet ($\delta \approx 3.3$ ppm in $CHCl_3$, 9H), which resides far away from solvent, porphyrin, and ligand proton resonances. While the χ_0 value of trimethylorthoformate to our knowledge has not been experimentally determined, a molar susceptibility of 50×10^{-6} mol/cm^3 ($\chi_0 \approx 4.72 \times 10^{-7}$ g/cm^3) was estimated from the molar susceptibilities of similar compounds listed in the *Handbook of Chemistry and Physics*, 74th ed. This standard comprised 2% of the total solvent volume in the inner and outer tubes in these experiments. Due to the necessity of using large excesses of axial ligand to guarantee a homogeneous coordination environment in these experiments (vide infra), the use of high (mM) (porphinato)iron(III) complex concentrations (to ensure large magnitude $\Delta\nu$ values) was precluded. In these experiments, the concentrations of paramagnetic complexes were ~0.7 mg/mL, which provided $\Delta\nu$ values on the order of 30 Hz, which were large enough to accurately measure at a field strength of 500 MHz.

(4-Formyl-phenoxy)acetic Acid Ethyl Ester (1). This precursor synthesis is analogous to that reported in the literature.[64] A 200-mL round-bottom flask was charged with of 4-hydroxybenzaldehyde (6.5 g, 53 mmol), ethyl bromoacetate (9.78 g, 58.5 mmol), potassium carbonate (8.08 g, 58.5 mmol), and 100 mL of acetone. The reaction mixture was brought to a gentle reflux overnight. It was then diluted with water and extracted thrice with ethyl ether. The combined ether layers were then washed three times with 2 M KOH solution and once with water. The organic layer was then dried over Na_2SO_4 and evaporated to yield a yellow oil (15.3 g, 90% yield based on the mass of 4-hydroxybenzaldehyde). ^{1}H NMR (250 MHz, $CDCl_3$): δ 9.88 (s, 1 H), 7.82 (d, 2 H, $J = 4.6$ Hz), 7.0 (d, 2 H, $J = 4.6$ Hz), 4.69 (s, 2 H), 4.25 (q, 2 H, $J = 7.0$ Hz), 1.25 (t, 3 H, $J = 7.0$ Hz). HRMS (M^+): 208.0734 (calcd 208.0735).

[5,15-Di((4-ethyl ester)methylene-oxy)phenyl]porphyrin (2). 2,2′-Dipyrrylmethane[65,66] (1.54 g, 10.5 mmol) and **1** (2.19 g, 10.5 mmol) were brought together in a 2-L round-bottom flask containing 1.5 L of dry methylene chloride and a magnetic stir bar under N_2. Trifluoroacetic acid (0.16 mL, 2.1 mmol) was added to this mixture; the flask was then covered with aluminum foil and stirred at room temperature for 14 h. DDQ (2,3-dichloro-4,5-dicyanoquinone, 3.58 g, 15.75 mmol) was added to the methylene chloride solution, and the mixture was allowed to stir for 15 min before the solvent was removed under reduced pressure. The reaction mixture was then purified by silica chromatography using 99:1 CH_2Cl_2/methanol as the eluant, to give 1.5 g of the isolated product (43% yield based on 1.54 g of the dipyrrylmethane starting material). Vis (CH_2Cl_2) λ_{max} nm (log ϵ): 408 (5.37), 504 (4.17), 539 (3.79), 577 (3.75), 632 (3.37). ^{1}H NMR (250 MHz, $CDCl_3$): δ 10.29 (s, 2 H), 9.37 (d, 4 H, $J = 4.65$ Hz), 9.07 (d, 4 H, $J = 4.65$ Hz), 8.16 (d, 4 H, $J = 7.95$ Hz), 7.28 (d, 4 H, $J = 7.95$ Hz) 5.53 (s, 4 H), 4.40 (q, 4 H, $J = 7.28$ Hz), 1.42 (t, 6 H, $J = 7.30$ Hz), −3.02 (broad s, 2 H). HRMS (MH^+): 667.2573 (calcd 667.2537).

5-Bromo-[10,20-di((4-ethyl ester)methylene-oxy)phenyl]porphyrin (3). In a 1.0-L round-bottomed flask, **2** (600 mg, 0.9 mmol) was dissolved in 500 mL of methylene chloride and cooled to 0 °C. *N*-Bromosuccinimide (128 mg, 0.72 mmol) was then added to the stirring porphyrin solution. After 15 min, the reaction was quenched by the addition of 30 mL of acetone. The solvents were removed, and the recovered residue was purified by silica chromatography using methylene chloride as the eluant. Three purple bands were observed; the second band was isolated as the desired product (369 mg, 68.7% yield based on 128 mg of NBS). Vis (CH_2Cl_2) λ_{max} (log ϵ): 417 (5.36), 513 (4.12), 549 (3.76), 590 (3.61) 646 (3.41). ^{1}H NMR (250 MHz, $CDCl_3$): δ 10.14 (s, 1 H), 9.70 (d, 2 H, $J = 4.875$ Hz), 9.25 (d, 2 H, $J = 4.7$ Hz), 8.90 (q, 4 H, $J = 4.6$), 8.1 (d, 4 H, $J = 8.75$ Hz), 7.3 (d, 4 H, $J = 8.55$ Hz), 5.30 (s, 4 H), 4.40 (q, 4 H, $J = 7.28$ Hz), 1.42 (t, 6 H, $J = 7.30$ Hz), −3.02 (broad s, 2 H). HRMS (MH^+): 745.1651 (calcd 745.1661).

5-Bromo-[(10,20-di((4-ethyl ester)methylene-oxy)phenyl)porphinato]zinc(II) (4). Compound **3** (250 mg, 0.34 mmol) and zinc acetate (735 mg, 3.35 mmol) were refluxed in chloroform (400 mL) in a 1-L round-bottom flask equipped with a magnetic stir bar and a reflux condenser. The reaction was monitored by electronic absorption spectroscopy and was complete within 2 h. Following evaporation of solvent, the residue was passed down a short silica column using methylene chloride as the eluent. The desired product eluted first and was collected in quantitative yield. Vis (CH_2Cl_2) λ_{max} (log ϵ): 418 (5.47), 547 (4.09), 586 (3.28). ^{1}H NMR (250 MHz, $CDCl_3$): δ 10.05 (s, 1 H), 9.70 (d, 2 H, $J = 4.7$ Hz), 9.24 (d, 2 H, $J = 4.4$ Hz), 8.9 (q, 4 H, $J = 4.6$ Hz), 8.0 (d, 4 H, $J = 7.95$ Hz), 7.26 (d, 4 H, $J = 7.95$ Hz) 4.89 (s, 4 H), 4.40 (q, 4 H, $J = 7.28$ Hz), 1.39 (t, 6 H, $J = 6.9$ Hz). HRMS (M^+): 806.0768 (calcd 806.0718).

5-Trimethylsilylethynyl-[(10,20-di((4-ethyl ester)methylene-oxy)-phenyl)porphinato]zinc(II) (5). Trimethylsilylacetylene (0.30 mL, 2.5 mmol) and 5 mL of THF were brought together in a 50-mL Schlenk tube. The solution was deaerated and cooled to −78 °C. *n*-Butyllithium (0.84 mL of a 2.5 M hexanes solution, 2.1 mmol) was added dropwise, following which the Schlenk tube was removed from the dry ice/acetone bath and slowly warmed to room temperature. A THF solution of zinc chloride (429 mg, 3.15 mmol) was cannula transferred into the solution containing the lithiated ethynyl(porphinato)zinc(II) compound, upon which the reaction mixture turned cloudy. A separate Schlenk tube was charged with **4** (170 mg, 0.21 mmol), $Pd(PPh_3)_4$ (24 mg, 0.021 mmol), and 30 mL of THF. After deaerating the porphyrin solution by three freeze−pump−thaw−degas cycles, the contents of both Schlenk tubes were combined and stirred in a 50 °C oil bath under N_2 overnight. The reaction mixture was then diluted with ethyl acetate and washed twice with NH_4Cl and once with water. The organic phase was dried over Na_2SO_4 and evaporated. The resulting mixture was purified via silica chromatography using 30% THF in hexanes as eluant. The fluorescent purple band was isolated, giving the desired product (165 mg, 86.8% yield based on 170 mg of compound **4**). Vis (CH_2Cl_2) λ_{max} (log ϵ): 425 (5.34), 555 (4.18), 596 (3.85) nm. ^{1}H NMR (250 MHz, $CDCl_3$):

(64) Lottner, C.; Bart, K.-C.; Bernhardt, G.; Brunner, H. *J. Med. Chem.* **2002**, *45*, 2079−2089.
(65) Lin, V. S.-Y.; Iovine, P. M.; DiMagno, S. G.; Therien, M. J.; Malinak, S.; Coucouvanis, D. *Inorg. Synth.* **2002**, *33*, 55−61.
(66) Littler, B. J.; Miller, M. A.; Hung, C.-H.; Wagner, R. W.; O'Shea, D. F.; Boyle, P. D.; Lindsey, J. S. *J. Org. Chem.* **1999**, *64*, 1391−1396.

δ 10.11 (s, 1 H), 9.76 (d, 2 H, J = 4.73 Hz), 9.27 (d, 2 H, J = 4.55 Hz), 9.00 (d, 2 H, J = 4.88 Hz), 8.98 (d, 2 H, J = 4.60 Hz), 8.11 (d, 4 H, J = 8.55 Hz), 7.30 (d, 4 H, J = 8.60 Hz), 4.91 (s, 4 H), 4.40 (q, 4 H, J = 7.23 Hz) 1.42 (t, 6 H, J = 7.15 Hz), 0.62 (s, 9 H).

5-Ethynyl-[(10,20-di((4-ethyl ester)methylene-oxy)phenyl)porphinato]zinc(II) (6). Compound **5** (165 mg, 0.182 mmol) was dissolved in 150 mL of a 1:1 THF/EtOH solution. Potassium carbonate (252 mg, 1.82 mmol) was added, and the reaction was stirred in the dark at ambient temperature overnight. Once the reaction was complete, the solvents were removed, and the recovered residue was purified by column chromatography via a short silica gel column using 3:2 hexanes/THF as the eluant. The fluorescent purple band was collected and concentrated. The resulting solid was further purified by recrystallization from THF/hexanes to give 125 mg of the title compound (82% yield, based on 165 mg of the (porphinato)zinc(II) starting material). Vis (CH_2Cl_2) λ_{max} (log ϵ): 422 (5.33), 552 (4.33), 591 (3.85) nm. ^{1}H NMR (250 MHz, 19:1 $CDCl_3$/d_5-pyridine): δ 10.15 (s, 1 H), 9.75 (d, 2 H, J = 4.82 Hz), 9.30 (d, 2 H, J = 4.75 Hz), 9.01 (d, 2 H, J = 4.41 Hz), 8.98 (d, 2 H, J = 4.41 Hz), 8.10 (d, 4 H, J = 8.53 Hz), 7.30 (d, 4 H, J = 8.78 Hz), 4.91 (s, 4 H), 4.40 (q, 4 H, J = 7.26 Hz), 4.13 (s, 1 H), 1.43 (t, 6 H, J = 7.13 Hz). ESI-MS (M^+): 752.10 (calcd 752.16).

[5-[(10,20-Di-((4-ethyl ester)methylene-oxy)phenyl)porphinato]-zinc(II)]−[5′-[(10′,20′-di-(4-ethyl ester)methylene-oxy)phenyl]porphyryl]ethyne (7). A 100-mL Schlenk tube was charged with **6** (70 mg, 0.084 mmol), **3** (75 mg, 0.101 mmol), triphenylarsine (50 mg, 0.164 mmol), the catalyst Pd_2dba_3 (19 mg, 0.021 mmol), and 50 mL of dry THF. Following the addition of 2 mL of triethylamine, the reaction was deaerated by three freeze−pump−thaw cycles and stirred at 35 °C under N_2 for 2 d. The solution was then diluted with EtOAc and washed thrice with water, and the combined organic layer was dried over $MgSO_4$. After the organic solvents were removed, the recovered green solid was purified by column chromatography on silica gel using 3:2 hexanes/THF as the eluant. Following elution of monomeric porphyrin species and a butadiyne-bridged (porphinato)-zinc(II) impurity, the eluant polarity was increased to 100% THF. The title compound was isolated and further purified by recrystallization from THF/hexanes to give pure **7** (85 mg, 71% yield based on 70 mg of the (porphinato)zinc(II) starting material). Vis (CH_2Cl_2) λ_{max} (log ϵ): 416 (5.33), 473 (5.31), 521 (4.32), 567 (4.30), 644 (4.39), 708 (4.55) nm. ^{1}H NMR (250 MHz, 19:1 $CDCl_3$/d_5-pyridine): δ 10.40 (d, 2H, J = 4.63 Hz), 10.35 (d, 2H, J = 4.63 Hz), 10.07 (s, 1 H), 10.05 (s, 1 H), 9.21 (t, 4 H, J = 4.10 Hz), 9.11 (d, 2 H, J = 4.65 Hz), 9.07 (d, 2 H, J = 4.80 Hz), 8.92 (t, 4 H, J = 4.48 Hz), 8.13 (m, 8 H), 7.26 (m, 8 H), 4.88 (s, 8 H), 4.37 (q, 8 H, J = 7.08 Hz), 1.35 (t, 12 H, J = 6.95 Hz), −2.27 (broad s, 2 H). MALDI-TOF MS (M^+): 1418.87 (calcd 1418.82).

5-[(10,20-Di-((4-ethyl ester)methylene-oxy)phenyl)porphinato]-zinc(II)−[5′-[(10′,20′-di-(((4-ethyl ester)methylene-oxy)phenyl)porphinato]iron(III)-chloride]ethyne (PZn−PFe-Cl) (8). 5-[(10,20-Di-(((4-ethyl ester)methylene-oxy)phenyl)porphinato]zinc(II)]−5′-(10′,20′-di-(((4-ethyl ester)methylene-oxy)phenyl)porphyryl)ethyne (10 mg, 0.007 mmol) was dissolved in 20 mL of ethanol and 60 mL of $CHCl_3$. Ferrous chloride tetrahydrate (7 mg, 0.035 mmol) was added to the stirring porphyrin solution, and the reaction was refluxed under N_2. The metal insertion reaction was monitored by electronic absorption spectroscopy and was complete after 2 h. The solvents were evaporated, and the recovered residue was loaded onto a short neutral alumina plug (Fluka, type H). The product was eluted with THF and concentrated. The recovered solid was then dissolved in CH_2Cl_2 and washed thrice with 1 M HCl and three times with water, and was dried over $CaCl_2$ and evaporated. Recrystallization of the isolated bis[(porphinato)metal]-complex from THF/hexanes gave 10 mg of compound **8** (quantitative yield). Vis (CH_2Cl_2) λ_{max} (log ϵ): 423 (4.96), 467 (4.92), 512 (4.35), 607 (4.30), 680 (4.15), 731 (4.08) nm. MALDI-TOF MS (M^+ − axial Cl^-): 1472.66 (calcd 1472.65).

[5-[(10,20-Di-((4-ethyl ester)methylene-oxy)phenyl)porphinato]-zinc(II)-pyridine]−[5′-[(10′,20′-di-((4-ethyl ester)methylene-oxy)-phenyl)porphinato]iron(II)-(pyridine)$_2$]ethyne (PZn−PFe-(py)$_2$). Mossy zinc (5 g, 76.5 mmol), previously washed with 0.1 N HCl and rinsed to neutral pH using deionized (DI) water, was placed in a 125-mL Erlenmeyer flask containing 25 mL of DI water. A solution of HgO (166 mg in ∼1 mL of concentrated HCl) was added dropwise to the mossy zinc with continuous swirling. Once H_2 evolution had ceased, the resulting Zn/Hg amalgam was filtered and rinsed thoroughly with DI water. The amalgam was then dried under vacuum for several hours. A 50-mL Schlenk-style round-bottomed flask equipped with a magnetic stir bar was charged with **PZn−PFe-Cl** and the Zn/Hg amalgam. Once the flask had been thoroughly deaerated, 10 mL of 10:1 C_6D_6/d_5-pyridine was added via cannula. The flask was warmed to 45 °C, and the reduction was allowed to proceed over 2 h. The solution was then filtered and transferred to a NMR tube under N_2. Optical and ^{1}H NMR data were consistent with homogeneous conversion of **PZn−PFe-Cl** to **[PZn−PFe-(py)$_2$]**. Vis (C_6D_6/pyridine-d_5, 10:1): 428, 476, 536, 572, 684 nm. ^{1}H NMR (360 MHz, C_6D_6/pyridine-d_5, 10:1): δ 10.8 (m, 4 H), 10.05 (s, 1 H), 9.55 (s, 1 H), 9.23 (m, 4 H), 9.20 (m, 4 H), 9.00 (m, 4 H), 8.10 (m, 8 H), 7.60 (m, 8 H), 4.55 (m, 8 H), 4.10 (m, 8 H), 1.46 (m, 12 H).

[5,15-Di[((4-ethyl ester)methylene-oxy)phenyl]porphinato]iron-(III)-chloride (PFe-Cl). Iron metalation of the free-base macrocycle followed a previously reported procedure.[67] Compound **2** (100 mg, 0.150 mmol), dissolved in 20 mL of EtOH and 60 mL of $CHCl_3$ with $FeCl_2$·$4H_2O$ (149 mg, 0.750 mmol), was refluxed under Ar for 2 h, during which time the color changed from purple to brown. After electronic absorption spectroscopy indicated the reaction was complete, the solvent was evaporated, and excess ferrous chloride salt was removed from the residue via chromatography on a short neutral alumina plug using THF as the eluant. The product, recovered as the μ-oxo-bridged bis[(porphinato)Fe(III)] complex, was dissolved in $CHCl_3$ and washed thrice with 1 M HCl using a separatory funnel, followed by three water washings. Following removal of chloroform, 105 mg of the desired product was isolated (93% yield, based on 100 mg of compound **2**). Vis (CH_2Cl_2) λ_{max} (log ϵ): 377(4.62), 408(4.81), 502-(4.03), 574(3.46), 641(3.40), 674(3.32) nm. FAB-MS (M^+ − axial Cl^-): 720.6 (calcd 720.2).

Determination of Ligand Binding Constants. Electronic absorption spectral changes were recorded upon the addition of known amounts of nitrogenous Lewis base to 5 × 10^{-5} M solutions of [5,15-di[((4-ethyl ester)methylene-oxy)phenyl]porphinato]iron(III)-chloride (**PFe-Cl**) in CH_2Cl_2. The solution was stirred vigorously after each addition of axial ligand. The change in total solution volume between the start and finish of these titration experiments was less than 10%. Equilibrium constants K_1 and β_2, as defined by eqs 4−6, were determined by methods established previously by Walker.[68,69]

$$\mathrm{PFeCl} + \mathrm{L} \overset{K_1}{\rightleftharpoons} \mathrm{PFeClL} \tag{4}$$

$$\mathrm{PFeClL} + \mathrm{L} \overset{K_2}{\rightleftharpoons} \mathrm{PFeL_2}^{+}\mathrm{Cl}^{-} \tag{5}$$

$$\mathrm{PFeCl} + 2\mathrm{L} \underset{\beta_2 = K_1K_2}{\overset{\beta_2}{\rightleftharpoons}} \mathrm{PFeL_2}^{+}\mathrm{Cl}^{-} \tag{6}$$

Results and Discussion

Synthesis. Using methodology described previously,[12,13,55,61,70] **PZn−PFe-Cl** was synthesized by the route outlined in Scheme

(67) Ikeue, T.; Ohgo, Y.; Saitoh, T.; Yamaguchi, T.; Nakamura, M. *Inorg. Chem.* **2001**, *40*, 3423−3434.
(68) Walker, F. A.; Lo, M.-W.; Ree, M. T. *J. Am. Chem. Soc.* **1976**, *98*, 5552−5560.
(69) Koerner, R.; Wright, J. L.; Ding, X. D.; Nesset, M. J. M.; Aubrecht, K.; Watson, R. A.; Barber, R. A.; Mink, L. M.; Tipton, A. R.; Norvell, C. J.; Skidmore, K.; Simonis, U.; Walker, F. A. *Inorg. Chem.* **1998**, *37*, 733−745.
(70) DiMagno, S. G.; Lin, V. S.-Y.; Therien, M. J. *J. Org. Chem.* **1993**, *58*, 5983−5993.

Scheme 1. Synthetic Route to **PZn−PFe−Cl**

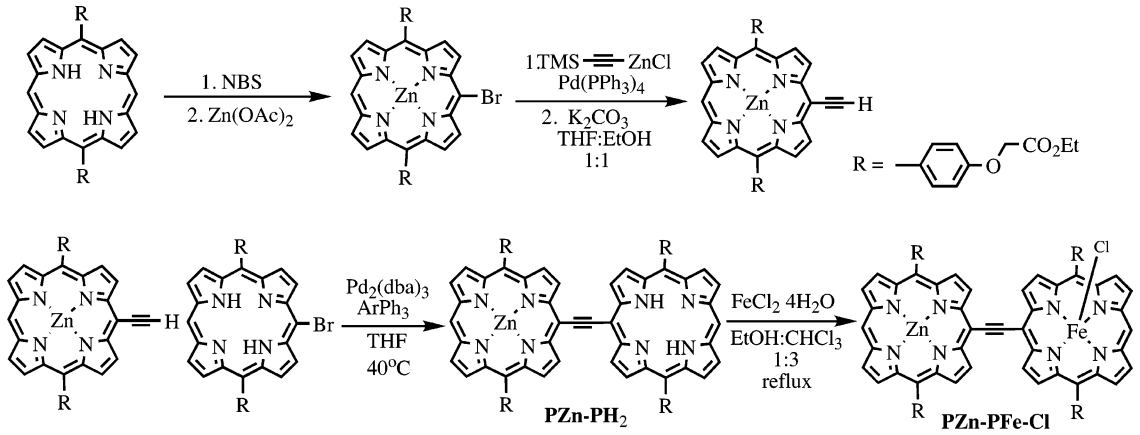

1. This synthesis of a *meso*-to-*meso* ethyne-bridged mixed-metal bis(porphyrin) complex utilized (5-ethynylporphinato)zinc(II) and 5-bromoporphyrin precursors (Scheme 1). This strategy avoids the presence of a redox-active, axially ligated metal center in the reductive metal-catalyzed cross-coupling reaction conditions, and produces an intermediate *meso*-to-*meso* ethyne-bridged (porphinato)zinc(II)−porphyrin (**PZn−PH$_2$**) compound[55] that can be isolated and characterized prior to subsequent metalation.[67]

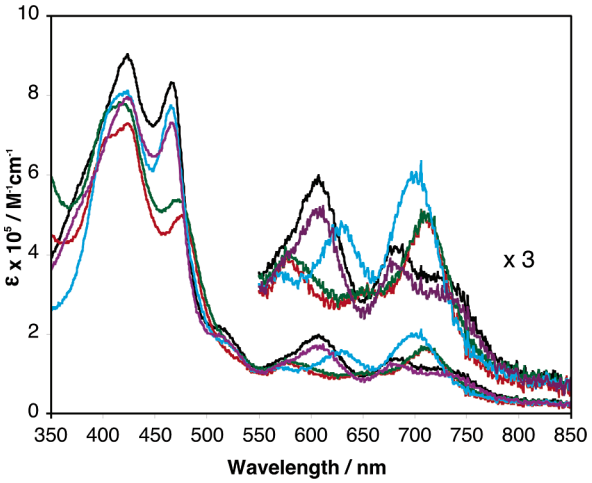

Figure 1. Ground-state electronic absorption spectra of **PZn−PFe-Cl** (black line) and **PZn−PFe-Cl** in the presence of 5000-fold molar excess of specific nitrogenous Lewis bases (L) in CH_2Cl_2 solvent [L = pyridine (blue line), 4-cyanopyridine (magenta line), collidine (red line), and 2,6-lutidine (green line)].

Ground-State Electronic Absorption Spectra. Figure 1 shows the electronic absorption spectrum of **PZn−PFe-Cl**. The gross spectral features of this complex resemble those delineated for *meso*-to-*meso* ethyne-bridged bis[(porphinato)zinc(II)] (**PZn−PZn**) compounds,[12,13,46,49,55,59,61,62] featuring two dominant absorption manifolds derived from the classic porphyrin B (Soret)- ($S_0 \rightarrow S_2$) and Q-band ($S_0 \rightarrow S_1$) transitions. It is noteworthy that the electronic absorption spectrum of **PZn−PFe-Cl** is not superimposable on the combined electronic absorption spectra of its monomeric precursors, reflecting the extensive interpigment excitonic interactions and extensive π electronic delocalization characteristic of this class of supermolecular chromophores. While the optical spectroscopic features of this class of highly conjugated bis(chromophore) structures have been discussed extensively,[12,13,46,49,55,61] a number of distinct characteristics of the **PZn−PFe-Cl** electronic absorption spectrum are worth noting. Relative to **PZn−PZn** species, **PZn−PFe-Cl** displays a Soret region absorption band maximum that is less intense than that manifested by its **PZn−PZn** counterpart. Further, the spectral breadth of the **PZn−PFe-Cl** S_2-state absorption manifold (fwhm $\approx$ 7000 cm^{-1}) exceeds that established for **PZn−PZn** ($\sim$4600 cm^{-1}).[12,13,46,49,55,61] In this regard, these S_2-state absorption manifold characteristics resemble those described for [(5,-10,20-bis[3,5-bis(3,3-dimethyl-1-butyloxy)phenyl]porphinato)zinc(II)]−[(5′,-15′-ethynyl-10′,-20′-bis[10,20-bis(heptafluoropropyl)]porphinato)zinc(II)]-ethyne,[61,62] an electronically asymmetric *meso*-to-*meso* ethyne-bridged bis[(porphinato)zinc(II)] complex, which is composed of a 10,20-aryl-substituted macrocycle and a second (porphinato)zinc(II) unit that features σ-electron-withdrawing perfluoropropyl groups at the 10 and 20 positions.[71] As in this previously studied electronically asymmetric highly conjugated bis[(porphinato)metal] complex,[61,62] **PZn−PFe-Cl** features a low-energy Q_x absorption band that is both broader and tails more significantly to the red, than that observed for **PZn−PZn**,[12,13,46,49,55,61,62] suggestive of increased charge-resonance character of this transition.

Mechanistic studies of electron transfer, as well as excitation delocalization and excitation migration processes in mixed-metal multiporphyrin systems have typically examined assemblies that feature spectroscopically identifiable chromophoric entities that function as energy donors and acceptors. For multi(porphinato)-metal systems that feature d^1-d^9 metal centers, the metal *d* manifold typically affords a multiplicity of states lower in energy than the (porphinato)zinc(II) S_1 state.[72−77] In weakly coupled (porphinato)zinc(II)−spacer−(porphinato)iron(III) (PZn−Sp−PFe) systems, both energy- and electron-transfer migration to

(71) While Fe *d* character is manifest in the ground- and excited-state wave functions, we utilize S_0, S_1, S_2, and S_n labels for these ground and initially prepared excited states to facilitate comparisons to the established spectroscopy and dynamics of closely related diamagnetic analogues of **PZn−PFe(III)**.

(72) Brookfield, R. L.; Ellul, H.; Harriman, A. *J. Chem. Soc., Faraday Trans. 2* **1985**, *81*, 1837−1848.
(73) Mataga, N.; Yao, H.; Okada, T.; Kanda, Y.; Harriman, A. *Chem. Phys.* **1989**, *131*, 473−480.
(74) Zaleski, J. M.; Chang, C. K.; Nocera, D. G. *J. Phys. Chem.* **1993**, *97*, 13206−13215.
(75) Zhou, X.; Chan, K. S. *J. Org. Chem.* **1998**, *63*, 99−104.
(76) Borovkov, V. V.; Lintuluoto, J. M.; Inoue, Y. *Helv. Chim. Acta* **1999**, *82*, 919−934.
(77) Kilså, K.; Kajanus, J.; Larsson, S.; Macpherson, A. N.; Mårtensson, J.; Albinsson, B. *Chem. Eur. J.* **2001**, *7*, 2122−2133.

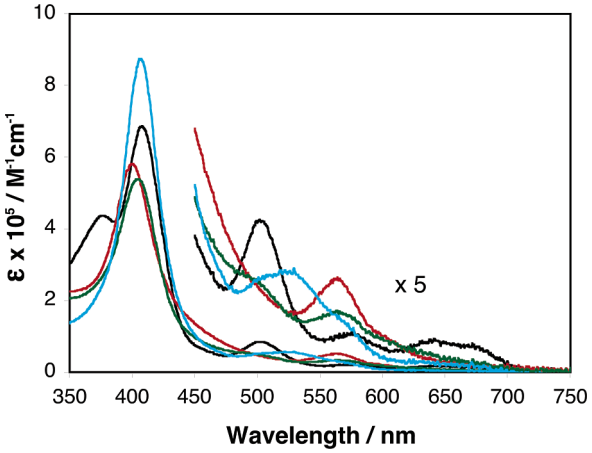

Figure 2. Ground-state electronic absorption spectra of **PFe-Cl** (black line) and **PFe-Cl** in the presence of 5000-fold molar excess of specific nitrogenous Lewis bases (L) in CH_2Cl_2 solvent [L = pyridine (blue line), collidine (red line), and 2,6-lutidine (green line)]. The spectrum for L = 4-cyanopyridine is omitted for clarity, as it is nearly identical to that for **PFe-Cl**.

the PFe(III) chromophore from the PZn-localized singlet excited state have been observed.[73,77−89] Such PZn−Sp−PFe assemblies have utilized hydrogen-bonded interfaces,[84] as well as rigid phenyl,[79−82,86,87] and (phenylethynyl)-arene[73,85,88,89] bridging moieties, to connect the porphyrin-based pigments; for such linkage motifs, excitation delocalization is negligible, as these Sp structures afford only weak electronic coupling between the two (porphinato)metal units.

Given the extensive pigment−pigment coupling driven by a *meso*-to-*meso* ethyne bridge, the nature of metal *d* manifold electronic states would be expected to play a major role in determining the dynamics of $[\mathbf{PZn-PFe\text{-}(ligand)_{1,2}}]^+$ excited states. Consistent with this, distinct spectral changes in the **PZn−PFe-Cl** electronic absorption spectrum are observed upon the addition of nitrogenous Lewis bases (Figure 1). These spectral changes are analogous to those observed for [5,15-di-[((4-ethyl ester)methylene-oxy)phenyl]porphinato]iron chloride (**PFe-Cl**; Figure 2) upon addition of identical ligating axial Lewis bases.[90−92] For instance, classic intensification of the Q-band α- and *β*-absorptions are clearly evident in Figures 1−2 upon pyridine ligation; such spectral changes are diagnostic of a bis-axially ligated (porphinato)iron(III) [PFe(III)] center.[90,92−94] 4-Cyanopyridine, a poor *σ*-donor, is known to have a minimal impact on **PFe-Cl** electronic spectral features;[91] congruent with this, the **PZn−PFe-Cl** spectrum is modulated little by the presence of large excesses of 4-cyanopyridine in solution (Figure 1). Likewise, substantial steric interactions between the porphyrin macrocycle and encumbered axial ligand substituents manifest predictable optical absorption spectral changes relative to the **PZn−PFe-Cl** spectrum. It has been demonstrated that axial metal ligation by bulky nitrogenous bases such as 2-*tert*-butylimidazole and 2-ethylimidazole effect a red-shift of the Q-band absorptions and intensification of an absorption band centered around 570 nm relative to that manifested for the corresponding ferric chloride complex;[92] these ligation-dependent electronic absorption spectral changes are mirrored in analogous experiments chronicled in Figure 2 for a benchmark **PFe(III)** complex and correspondingly bulky Lewis bases [collidine (2,4,6-trimethylpyridine) and 2,6-lutidine (2,6-dimethylpyridine)]. Bulky axial ligands related to collidine and 2,6-lutidine have been established to stabilize high-spin PFe(III) electronic states;[95,96] the Figure 1 and Figure 2 spectra suggest that, for PZn−PFe(III) compounds, these axial ligands drive similar high-spin Fe(III) electronic structures.

Nature of Collidine Ligation and the Resulting Spin State at Ferric Porphyrin Centers. The binding constants for a wide range of nitrogenous Lewis bases at ferrous and ferric porphyrin centers have been determined;[97] of the ligands highlighted in the spectra of Figures 1−2, only binding affinity data for collidine at PFe(III) sites remain sparse. While factors dictating ligation stoichiometry at PFe centers have been extensively studied,[68,97−100] cases where steric interactions play the dominant role in such interactions are few.[101,102] While it is well established that the ferrous ions of many biological hemes and *meso*-tetraphenylporphyrins (TPPs) are pentacoordinate with bulky axial ligands such as 2-methylimidazle[103−107] and 2,6-lutidine,[108] 2-methylimidazole has been shown to form a bis-axially ligated species at more sterically congested *meso*-(tetramesitylporphinato)iron(II) (TMPFe(II)).[101,102] Despite the established pentacoordinate binding stoichiometry of 2-methylimidazole, 1-methylbenzimidazole, and 2-methylpyrazines at TPPFe(II), these ligands nonetheless form hexacoordinated

(78) Fujita, I.; Netzel, T. L.; Chang, C. K.; Wang, C.-B. *Proc. Natl. Acad. Sci. U.S.A.* **1982**, *79*, 413−417.
(79) Meier, H.; Kobuke, Y.; Kugimiya, S. *Tetrahedron Lett.* **1989**, *30*, 5301−5304.
(80) Maruyama, K.; Osuka, A. *Pure Appl. Chem.* **1990**, *62*, 1511−1520.
(81) Osuka, A.; Maruyama, K.; Mataga, N.; Asahi, T.; Yamazaki, I.; Tamai, N. *J. Am. Chem. Soc.* **1990**, *112*, 4958−4959.
(82) Helms, A.; Heiler, D.; McLendon, G. L. *J. Am. Chem. Soc.* **1992**, *114*, 6227−6238.
(83) Tamiaki, H.; Nomura, K.; Maruyama, K. *Bull. Chem. Soc. Jpn.* **1994**, *67*, 1863−1871.
(84) de Rege, P. J. F.; Williams, S. A.; Therien, M. J. *Science* **1995**, *269*, 1409−1413.
(85) Osuka, A.; Tanabe, N.; Kawabata, S.; Yamazaki, I.; Nishimura, Y. *J. Org. Chem.* **1995**, *60*, 7177−7185.
(86) Chen, L. X.; Lee, P. L.; Gosztola, D.; Svec, W. A.; Montano, P. A.; Wasielewski, M. R. *J. Phys. Chem. B* **1999**, *103*, 3270−3274.
(87) Portela, C. F.; Brunckova, J.; Richards, J. L.; Schollhorn, B.; Iamamoto, Y.; Magde, D.; Traylor, T. G.; Perrin, C. L. *J. Phys. Chem. A* **1999**, *103*, 10540−10552.
(88) Kilså, K.; Macpherson, A. N.; Gillbro, T.; Mårtensson, J.; Albinsson, B. *Spectrochim. Acta, Part A* **2001**, *57*, 2213−2227.
(89) Pettersson, K.; Kilsa, K.; Martensson, J.; Albinsson, B. *J. Am. Chem. Soc.* **2004**, *126*, 6710−6719.
(90) Kobayashi, H.; Higuchi, T.; Kaizu, Y.; Osada, H.; Aoki, M. *Bull. Chem. Soc. Jpn.* **1975**, *48*, 3137−3141.
(91) Cheesman, M. R.; Walker, F. A. *J. Am. Chem. Soc.* **1996**, *118*, 7373−7380.
(92) Ikezaki, A.; Nakamura, M. *Inorg. Chem.* **2002**, *41*, 6225−6236.
(93) Robertson, D. E.; Farid, R. S.; Moser, C. C.; Urbauer, J. L.; Mulholland, S. E.; Pidikiti, R.; Lear, J. D.; Wand, A. J.; DeGrado, W. F.; Dutton, P. L. *Nature* **1994**, *368*, 425−432.
(94) Choma, C. T.; Lear, J. D.; Nelson, M. J.; Dutton, P. L.; Robertson, D. E.; DeGrado, W. F. *J. Am. Chem. Soc.* **1994**, *116*, 856−865.
(95) Bullard, L.; Panayappan, R. M.; Thorpe, A. N.; Hambright, P.; Ng, G. *Bioinorg. Chem.* **1974**, *3*, 161−164.
(96) Nakamura, M.; Nakamura, N. *Chem. Lett.* **1991**, 1885−1888.
(97) Walker, F. A.; Simonis, U. In *Encyclopedia of Inorganic Chemistry*; King, R. B., Ed.; Wiley & Sons: Chichester, U.K., 1994; Vol. 4, pp 1785−1846.
(98) Scheidt, W. R.; Reed, C. A. *Chem. Rev.* **1981**, *81*, 543−555.
(99) Momenteau, M.; Reed, C. A. *Chem. Rev.* **1994**, *94*, 659−698.
(100) Scheidt, W. R.; Lee, Y. J. *Struct. Bonding* **1987**, *64*, 1−70.
(101) Portela, C. F.; Magde, D.; Traylor, T. G. *Inorg. Chem.* **1993**, *32*, 1313−1320.
(102) Nesset, M. J. M.; Shokhirev, N. V.; Enemark, P. D.; Jacobson, S. E.; Walker, F. A. *Inorg. Chem.* **1996**, *35*, 5188−5200.
(103) Brault, D.; Rougee, M. *Biochem. Biophys. Res. Commun.* **1974**, *57*, 654−659.
(104) Wagner, G. C.; Kassner, R. J. *Biochim. Biophys. Acta* **1975**, *392*, 319−327.
(105) Wagner, G. C.; Kassner, R. J. *J. Am. Chem. Soc.* **1974**, *96*, 5593−5595.
(106) Collman, J. P.; Reed, C. A. *J. Am. Chem. Soc.* **1973**, *95*, 2048−2049.
(107) Ellison, M. K.; Schulz, C. E.; Scheidt, W. R. *Inorg. Chem.* **2002**, *41*, 2173-2181.
(108) Wang, C.-M.; Brinigar, W. S. *Biochemistry* **1979**, *18*, 4960−4977.

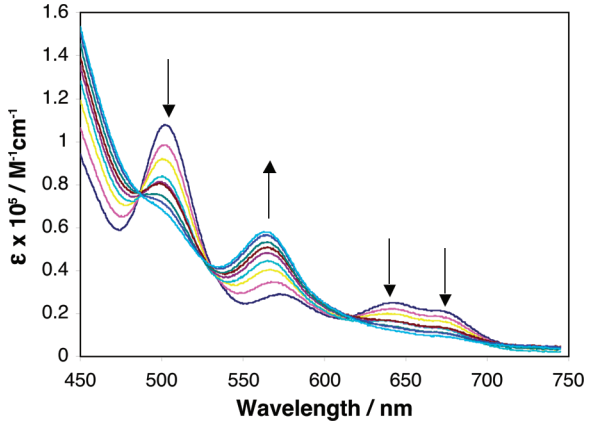

Figure 3. Collidine concentration dependent electronic absorption spectra for [5,15-di[((4-ethyl ester)methylene-oxy)phenyl]porphinato]iron(III) in CH_2Cl_2 solvent. Experimental conditions: [**PFe-Cl**] = 53 μM, T = 20 °C; [collidine]: 0 mM (black line), 26 mM (light red line), 52 mM (yellow line), 83 mM (blue-green line), 103 mM (magenta line), 127 mM (dark red line), 170 mM (green line), 200 mM (dark blue line), 311 mM (light blue line).

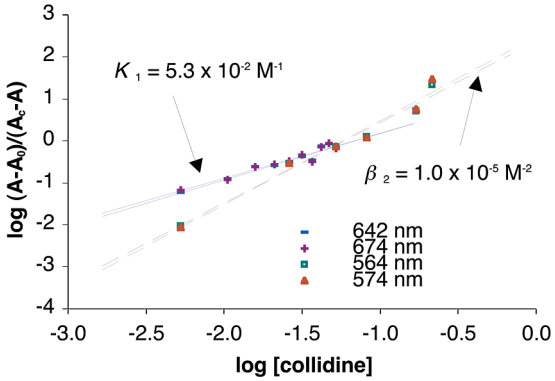

Figure 4. Determination of binding constants K_1 and β_2 for collidine at [5,15-di[((4-ethyl ester)methylene-oxy)phenyl]porphinato]iron(III). Experimental conditions: [**PFe-Cl**] = 53 μM, solvent = CH_2Cl_2, T = 20 °C.

Table 1. Equilibrium Ligand Binding Constants Determined for Nitrogenous Bases at (Porphinato)Iron(III) Centers via Electronic Absorption Spectroscopy[a]

PFe(III) complex	base	pK_a	solvent	log K_1 (M^{-1})	log β_2 (M^{-2})
PFe-Cl	collidine	7.43	CH_2Cl_2	−1.3	−5.0
TPPFe-Cl[68]	2-Me-Im	7.56	CH_2Cl_2	1.3	3.6
TPPFe-Cl[68]	N-Me-Im	7.33	CH_2Cl_2	1.9	4.0
TPPFe-Cl[68]	pyridine	5.28	$CHCl_3$	−0.7	−0.3

[a] [porphyrin] ≈ 10^{-5} M; experimental data obtained at ambient temperature; Im = imidazole.

species at TPPFe-(III);[109−112] similarly, contrary to simple expectations based on established axial ligation at TMPFe(II), TMPFe(III) centers with one axially ligated imidazole have been characterized.[92]

With respect to respect to encumbered pyridyl axial ligands, a 1:1 adduct of 2,6-dimethylpyridine with ferric protoporphyrin IX (PPIXFe) has been characterized in the solid state;[95] likewise, within a protoheme dimethylester ligand environment, ligand titration experiments show Fe(II) binds 2,6-lutidine in a 1:1 stoichiometry.[108] However, similar studies by Momenteau suggests that TPPFe(II) manifests hexacoordination in the presence of excess 2,6-lutidine.[113] Given these limited and perhaps contradictory observations regarding the role played by ligand steric factors in determining heme coordination environments, axial ligand titration studies were carried out to determine the nature of 2,6-dimethylpyridyl adducts at PFe(III); Figure 3 shows the Q-band region electronic absorption spectral changes that accompany increasing equivalents of collidine ligand added to a CH_2Cl_2 solution of **PFe-Cl**. Clear isosbestic behavior is observed at 486 nm (Figure 3). Crossover points centered around 530 and 615 nm spread over an approximate 10-nm range as collidine concentration is steadily increased (Figure 3); these spectral features resemble those observed previously for titrations involving other hindered bases[68] at PFe(III) complexes. Similar [collidine]-dependent spectral changes are observed in analogous titrations involving CH_2Cl_2 solutions of **PZn−PFe-Cl** (data not shown).

Collidine ligand binding equilibrium constants were determined from data analyzed using eqs 4−6 (Experimental Section); plots of $\log((A - A_0)/(A_c - A))$ vs log[L] were constructed. Here, A is the absorbance at the wavelength of interest, A_0 is the absorbance in the absence of ligand, A_c is that of the fully ligated complex, and [L] is the ligand concentration. Such plots, fashioned at four wavelengths, are shown in Figure 4. The formation constant of the pentacoordinated species, $-\log K_1$, was determined from the intercept of wavelength-dependent $\log((A - A_0)/(A_c - A))$ vs log[L] plots which displayed a linear relationship and a slope of unity; similarly, $-1/2 \log \beta_2$ was evaluated from wavelength-dependent linear $\log((A - A_0)/(A_c - A))$ vs log[L] relationships that displayed slopes of two. This analysis of the Figure 4 data gives $K_1 = 5.3 \times 10^{-2}$ M^{-1} and $\beta_2 = 1.0 \times 10^{-5}$ M^{-2}. Comparative equilibrium constants for ligand binding at PFe(III) are listed in Table 1. Note that the β_2 value evaluated for collidine at PFe(III) is ∼5 and 9 orders of magnitude smaller, respectively, than that determined for pyridine and 2-methylimidazole,[68,114] despite the fact that the 2,4,6-trimethylpyridine (collidine) pK_a value is comparable to those of the imidazole ligands. These data thus indicate that unlike the case for the binding of unencumbered pyridyl ligands to the PFe(III) centers of simple *meso*-arylporphyrins, ferric porphyrin centers remain nearly exclusively pentacoordinate throughout the collidine concentration regimes chronicled in the Figure 4 data.

The magnetic moment determined by Hambright for solid-state samples of PPIXFe(III)−(2,6-dimethylpyridine) and PPIXFe(III)−(2,4-dimethylpyridine) indicate a high-spin ferric heme at ambient temperature.[95] While these studies suggest a common $S = {}^5/_2$ spin state for pentacoordinate hemes featuring sterically encumbered, methyl-substituted pyridine and imidazole Lewis bases at ambient temperature, recent work demonstrates that the magnetic properties of such PFe(III)−L species are sensitive to solvent, temperature, and ligand electronic structure.[92] Extensive experimental data compiled by Nakamura for a series of (porphinato)Fe(III)−(imidazole) compounds show that the quantum mechanical spin-admixed state of high and intermediate

(109) Scheidt, W. R.; Kirner, J. F.; Hoard, J. L.; Reed, C. A. *J. Am. Chem. Soc.* **1987**, *109*, 1963−1968.
(110) Satterlee, J. D.; La Mar, G. N.; Bold, T. J. *J. Am. Chem. Soc.* **1977**, *99*, 1088−1093.
(111) Satterlee, J. D.; La Mar, G. N.; Frye, J. S. *J. Am. Chem. Soc.* **1976**, *98*, 7275−7282.
(112) Walker, F. A.; Reis, D.; Balke, V. L. *J. Am. Chem. Soc.* **1984**, *106*, 6888−6898.
(113) Momenteau, M.; Lavalette, D. *J. Am. Chem. Soc.* **1978**, *100*, 4322−4324.
(114) Coyle, C. L.; Rafson, P. A.; Abbott, E. H. *Inorg. Chem.* **1973**, *12*, 2007−2010.

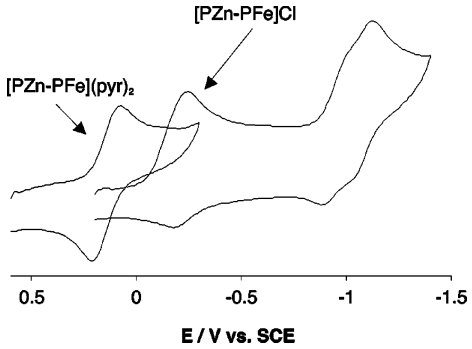

Figure 5. Cyclic voltammetric responses of **PZn−PFe-Cl** and **PZn−PFe-(pyridine)$_2$** recorded in methylene chloride solvent highlighting the reversible $Fe^{III/II}$ redox couples. Experimental conditions are described in Table 2.

spins ($S = {}^5/_2$ and $S = {}^3/_2$) can be accessed at ambient temperature.[92] For example, magnetic moments determined at 25 °C for a series of sterically encumbered TMPFe(III)−(L) compounds (L = 2- or 5-substituted imidazole) show that the $S = {}^3/_2$ contribution to the admixed spin state can range from 1 to 70% as function of the imidazole substituents. Further, the $S = {}^3/_2$ contribution to the admixed spin state was established to be sensitive to solvent polarity, diminishing precipitously with decreasing solvent dielectric strength.[92,115] Given the macrocycle electronic characteristics and axial ligand σ-donor and steric properties, these data raise the possibility that **[PFe-(collidine)]**$^+$ exists in the quantum mechanical spin-admixed ($S = {}^3/_2, {}^5/_2$) state at ambient temperature[92,95,115,116] with a spin composition dependent upon solvent polarity (vide infra). To ascertain the spin state of the pentacoordinate **[PFe-(collidine)]**$^+$, a series of NMR experiments was carried out to determine its magnetic moment. Using the experimental protocol established by Evans,[63] the monocollidine ligated ferric porphyrin center was determined to exist solely as a high spin species ($S = {}^5/_2$) at ambient temperature in chloroform solvent.

Cyclic Voltammetric Studies Probing the $Fe^{II/III}$ Redox Couple. Representative cyclic voltammetric responses recorded in CH_2Cl_2 solvent for **PZn−PFe** compounds are shown in Figure 5. The current vs potential profiles are consistent with previously investigated iron porphyrin species at solid working electrodes.[117−120] Table 2 lists the $E_{1/2}$ ($Fe^{II/III}$) values determined for **TPPFe** and **PZn−PFe** structures as a function of the (porphinato)iron axial ligand. Note that for all the PFe axial ligands examined in this study, the $E_{1/2}$ ($Fe^{II/III}$) value determined for a given Fe-ligated conjugated bis(porphyrin) compound, **PZn−PFe**, is ∼100 mV more positive than that exhibited by its corresponding **TPPFe-(ligand)$_{1,2}$** benchmark; thus, with respect to the Fe center, the (5-ethynylporphinato)zinc(II) moiety behaves as an electron-withdrawing substituent. As previously observed for **TPPFe** compounds (Table 2),[102,121] the $E_{1/2}$($Fe^{II/III}$) values determined for **PZn−PFe** species decrease with increasing acidity of the ligating pyridyl Lewis base.

Table 2. Comparative Cyclic Voltammetric Data for TPPFe and PZn−PFe Systems[a]

		potential (V)		
		$E_{1/2}(Fe^{II/III})$	$E_{1/2}(Fe^{II/III})$	$\log(K_{Fe(III)}/K_{Fe(II)})^b$
axial ligand	pK_a	TPPFe	PZn–PFe	PZn–PFe
Cl^-		−0.300[121]	−0.215	
collidine[c]	7.43	−0.260[122]	−0.170	−0.30
pyridine[c]	5.28	0.050[120]	0.145	−6.2
4-CNpy[c]	1.86	0.300[121]	0.385	−10

[a] Experimental conditions: [**PZn−PFe**] = 1 mM; [TBAP] = 0.1 M; [axial ligand] = 1 M; solvent = CH_2Cl_2; scan rate = 100 mV/s; working electrode = Pt disk. Potentials reported are relative to SCE. [b] Binding constants calculated as described by Kadish.[119,123] [c] Generated from the corresponding ferric chloride complex.

As Kadish has shown previously,[118,119,123,124] the relative pyridine binding affinities for PFe^{II} and PFe^{III} species can be evaluated from potentiometric data obtained as a function of exogenous axial ligand concentration. This relationship between ligand concentration and redox potential can be expressed in a modified version of the Nernst equation (eq 7):

$$(E_{1/2})_s = (E_{1/2})_c - \frac{n}{0.059}\log\left[\frac{K_{Fe(III)}}{K_{Fe(II)}}\right] - \frac{n}{0.059}\log\,[L]^{p-q} \quad (7)$$

Here, $(E_{1/2})_s$ and $(E_{1/2})_c$ are half wave reduction potentials of the fully ligated and ligand-free species, n is the number of electrons transferred, $K_{Fe(III)}$ and $K_{Fe(II)}$ are the formation constants of the ligated ferric and ferrous species, [L] is the ligand concentration, and p and q are number of ligands bound to the oxidized and reduced species, respectively.[119] The magnitude of the potential difference between the $Fe^{II/III}$ redox couples for high- and low-spin Fe^{III} species (determined from the reductive electrochemistry of the **PZn−PFe-Cl** and [**PZn−PFe-(ligand)$_{1,2}$**]$^+$ complexes) allows the evaluation of the ratio of the Fe(II) and Fe(III) axial ligand binding constants (Table 2). This analysis indicates that, for these pyridyl ligands, ferrous center stability correlates with the axial Lewis base pK_a value. Note also that the relative preference for maintaining a bis-axially ligated ferrous center for the 4-cyanopyridine ligand (Table 2) is 4 orders of magnitude greater [log(KFe(II)/KFe(III)) = 10] than that for pyridine [log(KFe(II)/KFe(III)) = 6.2]. The fact that the singly axial ligated collidine stabilizes poorly the ferrous porphyrin center relative to sterically unencumbered pyridyl ligands correlates with the low evaluated formation constant for bis-ligand coordination (Table 1).

Excited-State Dynamics of [PZn−PFe-(L)$_{1,2}$]$^+$ Chromophores. Pump−probe transient absorption spectroscopy was employed to examine the impact of axial ligation and solvent upon [**PZn−PFe(L)$_{1,2}$**]$^+$ excited-state relaxation dynamics. Representative transient absorption spectra obtained for **PZn−PFe-Cl** in methylene chloride solvent recorded at several time delays are shown in Figure 6. The early time spectrum (t_{delay} = 400 fs) displays four pronounced features: (i) a high oscillator strength bleach in the Soret ($S_0 \rightarrow S_2$) band region, (ii) a transient absorption between the Soret and x-polarized Q-state ($S_0 \rightarrow S_1$) transition in the ∼500−650 nm spectral domain (partially

(115) Sakai, T.; Ohgo, Y.; Hoshino, A.; Ikeue, T.; Saitoh, T.; Takahashi, M.; Nakamura, M. *Inorg. Chem.* **2004**, *43*, 5034−5043.
(116) Quinn, R.; Nappa, M.; Valentine, J. S. *J. Am. Chem. Soc.* **1982**, *104*, 2588−2595.
(117) Kadish, K. M.; Morrison, M. M.; Constant, L. A.; Dickens, L.; Davis, D. G. *J. Am. Chem. Soc.* **1976**, *98*, 8387−8390.
(118) Bottomley, L. A.; Kadish, K. M. *Inorg. Chem.* **1981**, *20*, 1348−1357.
(119) Kadish, K. M. In *Iron Porphyrins*; Lever, A. B. P., Gray, H. B., Eds.; Addison-Wesley: MA, 1983; Vol. 2, pp 161−249.
(120) Moore, K. T.; Fletcher, J. T.; Therien, M. J. *J. Am. Chem. Soc.* **1999**, *121*, 5196−5209.
(121) Kadish, K. M.; Bottomley, L. A. *Inorg. Chem.* **1980**, *19*, 832−836.
(122) Baker, J. A. ; University of Pennsylvania: Philadelphia, PA, 2000; p 241.
(123) Kadish, K. M.; Bottomley, L. A.; Beroiz, D. *Inorg. Chem.* **1978**, *17*, 1124−1129.
(124) Kadish, K. M.; Bottomley, L. A. *J. Am. Chem. Soc.* **1977**, *99*, 2380−2382.

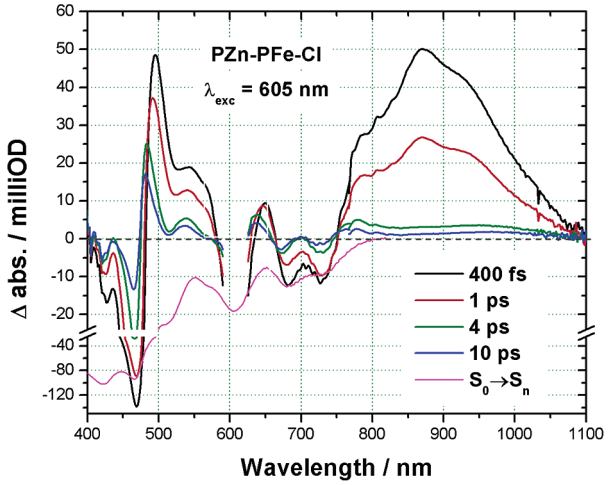

Figure 6. **PZn−PFe-Cl** transient absorption spectra determined at magic angle polarization; delay times = 0.4, 1.0, 4.0, and 10 ps. Experimental conditions: solvent = methylene chloride, λ_{ex} = 605 nm. A scaled steady-state absorption spectrum is shown inverted (solid pink line) for comparative purposes.

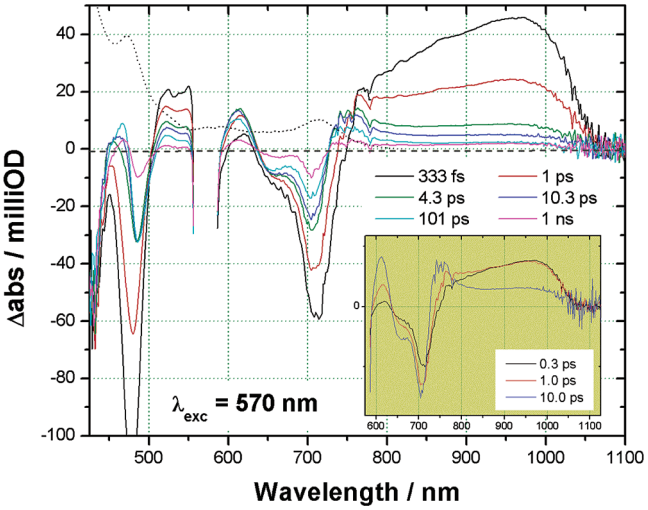

Figure 7. **[PZn−PFe-(collidine)]**$^+$ transient absorption spectra determined at magic angle polarization; delay times = 0.33, 1.0, 4.3, 10.3, 101, and 1000 ps. Experimental conditions: solvent = 10:1 CH_2Cl_2/collidine, λ_{ex} = 570 nm. A scaled steady-state absorption spectrum is shown (dotted line) for comparative purposes. (Inset) Transient absorption spectra normalized to the Soret band bleaching signature at delay times of 0.3, 1.0, and 10.0 ps showing the clear growth of a transient feature centered at approximately 680 nm.

obscured by scattering from the 605 nm excitation pump pulse), (iii) a bleach in the Q-band region, and (iv) an intense near-infrared (NIR) transient $S_1 \rightarrow S_n$ (λ_{max}: **PZn−PFe-Cl** ($S_1 \rightarrow S_n$) ≈ 870 nm; S_n = a higher-lying delocalized singlet excited state) that possess an integrated oscillator strength of magnitude comparable to the B- and Q-state bleaching transitions.[71] This low-energy feature of the **PZn−PFe-Cl** excited-state absorption spectrum resembles that manifested by *meso*-to-*meso* ethyne-bridged bis[(porphinato)zinc(II)] (**PZn−PZn**) compounds.[62] The intense, broad NIR $S_1 \rightarrow S_n$ transient absorption manifold is a spectroscopic hallmark of this class of highly conjugated multichromophoric compounds:[62,125,126] these excited-state transient absorption signatures are unique to strongly coupled bis-[(porphinato)metal] chromophores, and underscore the globally delocalized nature of the low-lying excited states of these systems.[62] Relative to the $S_1 \rightarrow S_n$ transient absorption manifold interrogated for bis[(5,5′-10,20-bis[3,5-bis(3,3-dimethyl-1-butyloxy)phenyl]porphinato)zinc(II)]ethyne (λ_{max}: **PZn−PZn** ($S_1 \rightarrow S_n$) ≈ 985 nm; fwhm = 655 cm^{-1}),[62] the **PZn−PFe-Cl** ($S_1 \rightarrow S_n$) manifold is significantly broader (fwhm = 2700 cm^{-1}), signaling a substantial charge resonance contribution to this transition.

Following excitation at 605 nm, the **PZn−PFe-Cl** transient absorption spectrum decays within several picoseconds back to the ground-state. The dynamics of the **PZn−PFe-Cl** excited-state decay are multiexponential, with the two largest amplitude decay component time constants possessing lifetimes of τ = 400 fs and 1.4 ps, though these values may reflect averages of several additional components. Note that the transient absorption spectrum recorded at 10 ps time delay shows evidence for a hot ground-state transition centered at ∼500 nm (Figure 6); this absorption decays with an 18 ps time constant. None of the fast excited-state decay components are associated with significant changes to the spectral shape of the transient signals, as indicated by the clear isosbestic point behavior at ΔA = 0 mOD, the corresponding decay-associated spectra (see Supporting Information), and the fact that spectra recorded at 0.4 and 1 ps are essentially superimposable (Figure 6) when normalized to uniform ΔA amplitude. These **PZn−PFe-Cl** excited-state dynamics are distinct from those delineated for **PZn−PZn** chromophores,[49,62,125] which are characterized by S_1-state lifetimes of ∼1 ns; in this regard, the **PZn−PFe-Cl** excited-state lifetime bears similarity to those determined for simple monomeric **PFe(III)** compounds (vide infra), where the partially filled ferric ion *d*-orbital shell gives rise to a multiplicity of states that facilitate subpicosecond and picosecond time scale deactivation of the initially prepared electronically excited state (Supporting Information).[127−129] Congruent with this picture, pump−probe transient absorption spectra acquired following electronic excitation of **[PZn−PFe-(py)$_2$]**$^+$ and **[PZn−PFe-(4-CN-py)$_2$]**$^+$ (see Supporting Information) feature NIR $S_1 \rightarrow S_n$ absorption manifolds and excited-state decay time constants nearly identical to those described above for **PZn−PFe-Cl**. The data shown in Figure 6 and in the Supporting Information for **PZn−PFe-Cl**, **[PZn−PFe-(py)$_2$]**$^+$, and **[PZn−PFe-(4-CN-py)$_2$]**$^+$ thus suggest that the **PZn−PFe** $E_{1/2}$ ($Fe^{II/III}$) value (Table 2), which varies by more than 600 mV in these three strongly conjugated bis[(porphinato)metal] compounds, exerts little influence on the observed excited-state dynamical behavior.

Excited-state dynamical data obtained following electronic excitation of **[PZn−PFe-(collidine)]**$^+$, however, challenge this simplistic picture. Transient absorption spectral data obtained for this compound in 10:1 CH_2Cl_2/collidine are shown in Figure 7. Note that the early time spectrum (t_{delay} = 300 fs) displays a NIR transition manifold (λ_{max} = 970 nm) significantly red-shifted (ΔE = 1185 cm^{-1}) with respect to the **PZn−PFe-Cl** NIR transient signal λ_{max} shown in Figure 6. The **[PZn−PFe-(collidine)]**$^+$ NIR excited-state transition manifold exhibits significant spectral breadth, ranging from ∼750 to 1050 nm; the fwhm of this manifold (>3500 cm^{-1}) exceeds that for the analogous transient absorption of electronically excited **PZn−PFe-Cl** by over 800 cm^{-1} (Figures 6 and 7). These facts, coupled with the observation that the **[PZn−PFe-(collidine)]**$^+$

(125) Duncan, T. V.; Susumu, K.; Sinks, L. E.; Therien, M. J. *J. Am. Chem. Soc.* **2006**, *128*, 9000−9001.
(126) Susumu, K.; Duncan, T. V.; Therien, M. J. *J. Am. Chem. Soc.* **2005**, *127*, 5786−5195.

and **PZn−PFe-Cl** excited-state NIR transition manifolds exhibit disparate spectral shapes, suggest that electronically excited **[PZn−PFe-(collidine)]**$^+$ possesses augmented charge resonance character as well as additional distinct underlying transitions within its NIR $S_1 \rightarrow S_n$ absorption manifold relative to that observed for electronically excited **PZn−PFe-Cl** (Figure 6).

The Figure 7 transient absorption spectral data obtained for **[PZn−PFe-(collidine)]**$^+$ possess two further striking aspects. The first includes the clear formation of a transient absorption band centered at approximately 680 nm during the first few picoseconds following photoexcitation. While this feature is partially obscured by the $S_0 \rightarrow S_1$ (Q-state) band bleaching signature, distinct rising signals are evident in the tailing regions of the $S_0 \rightarrow S_1$ bleach at ~620 and 740 nm. Growth of the transient signals at 620 and 740 nm occurs with concomitant loss of intensity in the transient NIR absorption band; normalized spectra highlighting this fact are shown in the Figure 7 inset. The dynamics of the growth and decay of this feature are multiexponential, but a global fit of the dynamics yield major decay constants of $\tau_1 \approx 0.3$ ps, $\tau_2 \approx 1.3$ ps, and $\tau_3 \approx 878$ ps (probe-wavelength-dependent relative amplitudes: $\lambda_{probe} = 950$ nm, $A(\tau_1):A(\tau_2):A(\tau_3) \approx 1:1:0$; $\lambda_{probe} = 620$, $A(\tau_1):A(\tau_2):A(\tau_3) \approx 1:1:-2$). The dynamics associated with the τ_1 relaxation time effect a substantial (~50%) diminution of the $S_1 \rightarrow S_n$ NIR transition moment and a concomitant rise in the transient absorption band centered at ~680 nm (Supporting Information, Figure S3); the dynamics associated with τ_2 primarily contribute to ground-state recovery, as the decay associated spectrum connected with this process is similar in shape to the ground-state bleaching signature. Consequently, the remaining 50% of the initial NIR transient absorption intensity decays via the τ_2 process. The ~880 ps characteristic relaxation time corresponds to the intrinsic decay time constant of the 680 nm-absorbing state back to the ground-state. Additional decay components with time constants of 13 and 96 ps, respectively, are evident but possess small associated amplitudes; both components contribute to a red-shift of the ground-state bleaching signature after formation of the absorption feature centered at 680 nm (Figure S3). Given the similarity of these time-dependent spectral changes and their associated time constants to established processes relevant to the excited-state dynamics of related **PZn−PZn** compounds,[62] these small amplitude decay components are likely associated with dynamics that lead to enhanced PZn-to-PFe conjugation (i.e., torsional relaxation around the ethyne bridge).

Given the observed spectral characteristics of the 680 nm transient absorption band and substantial literature precedent, this signal is assigned to a (porphinato)zinc(II) cation radical.[130,131,132] Of the two fastest dynamical components obtained from a global analysis of the transient spectral data, only τ_1 contributes significantly to the growth of the 680 nm transient absorption feature, and thus a charge separation time constant of 0.3 ps is concluded. The τ_2 time constant corresponds to the nonradiative decay of the initially prepared excited-state directly back to the ground-state, presumably via empty low-lying metal-centered states. Considering the difference in magnitude between τ_1 and τ_2, and the therefore disproportionably modest yield of the electron-transfer product (~50%) relative to the ground electronic state following internal conversion, it is reasonable to conclude that excited-state spectral dynamics following photoexcitation do not arise from a homogeneous excited-state

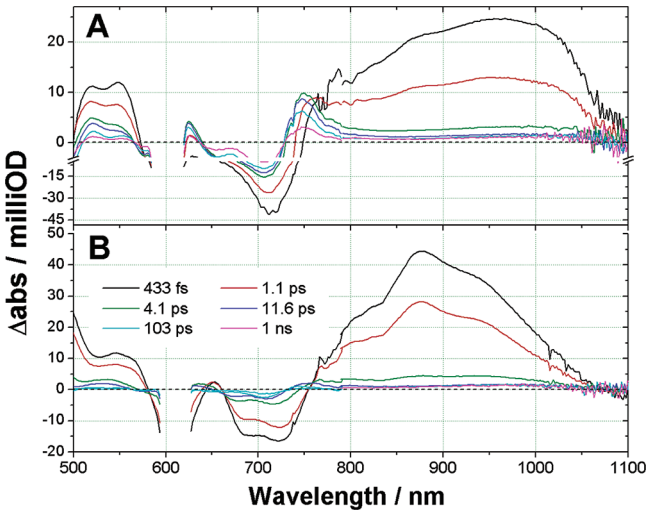

Figure 8. **[PZn−PFe-(collidine)]**$^+$ transient absorption spectra determined at magic angle polarization in (A) 10:1 benzonitrile/collidine and (B) 10:1 toluene/collidine; delay times = 0.43, 1.1, 4.3,11.6, 103, and 1000 ps, λ_{ex} = 605 nm.

population, as only a fraction of electronically excited **[PZn−PFe-(collidine)]**$^+$ species relax via an electron-transfer pathway. It should be noted that while the photoinduced charge separation time constant is close to the experimentally determined longitudinal relaxation times of methylene chloride ($\tau_L = 0.33$ and 0.56 ps),[133,134] identical experiments that probe **[PZn−PFe-(collidine)]**$^+$ excited states in benzonitrile solvent ($\tau_L = 6.9$ and 5.1 ps) evince almost identical excited-state relaxation dynamics (vide infra). We thus conclude that either (i) solvent relaxation dynamics have only a minimal effect on the excited-state decay processes of **[PZn−PFe-(collidine)]**$^+$ or (ii) the local chromophore solvation environment is dominated by collidine, which makes up 10% of the solvent mixture in these experiments, thereby masking dynamics associated with longitudinal CH_2Cl_2/benzonitrile relaxation.

In contrast to **PZn−PFe-Cl**, **[PZn−PFe-(py)$_2$]**$^+$, and **[PZn−PFe-(4-CN-py)$_2$]**$^+$ which evince subpicosecond and picosecond time-scale relaxation of their respective initially prepared electronically excited states to the ground state, **[PZn−PFe-(collidine)]**$^+$ excited-state dynamics show ultrafast relaxation to a $[(PZn-P)^{+\bullet}\ Fe^{II}-(collidine)]^+$ charge-separated state having a lifetime of nearly 1 ns. Figure 8 displays complimentary transient absorption spectral data obtained for **[PZn−PFe-(collidine)]**$^+$ in 10:1 benzonitrile/collidine and 10:1 toluene/collidine. **[PZn−PFe-(collidine)]**$^+$ excited-state dynamics evident in the benzonitrile solution (Figure 8A) resemble qualitatively those determined in the methylene chloride solution (Figure 7). Fast ($t \approx 1$ ps) loss of the NIR $S_1 \rightarrow S_n$ transition manifold

(127) Cornelius, A. W.; Steele, R. M.; Chernoff, D. A.; Hochstrasser, R. M. *Chem. Phys. Lett.* **1981**, *82*, 9−14.
(128) Adar, F.; Gouterman, M.; Aronowitz, S. *J. Phys. Chem.* **1976**, *80*, 2184−2191.
(129) Lim, M.; Jackson, T. A.; Anfinrud, P. A. *J. Phys. Chem.* **1996**, *100*, 12043−12051.
(130) Kang, Y. K.; Rubtsov, I. V.; Iovine, P. M.; Chen, J.; Therien, M. J. *J. Am. Chem. Soc.* **2002**, *124*, 8275−8279.
(131) Redmore, N. P.; Rubtsov, I. V.; Therien, M. J. *J. Am. Chem. Soc.* **2003**, *125*, 8769−8778.
(132) Fajer, J.; Borg, D. C.; Forman, A.; Dolphin, D.; Felton, R. H. *J. Am. Chem. Soc.* **1970**, *92*, 3451−3459.
(133) Grampp, G.; Landgraf, S.; Rasmussen, K. *J. Chem. Soc., Perkin Trans. 2* **1999**, 1897−1899.
(134) Horng, M. L.; Gardecki, J. A.; Papazyan, A.; Maroncelli, M. *J. Phys. Chem.* **1995**, *99*, 17311−17337.

intensity occurs concomitantly with the growth in the cation-radical feature centered at 680 nm. As in 10:1 methylene chloride/collidine solution, the **[PZn−PFe-(collidine)]**$^{+*}$ dynamics in 10:1 benzonitrile/collidine are multiexponential; analyses of these data reveal t_1, t_2, and t_3 time constants nearly identical in magnitude to those determined in 10:1 CH_2Cl_2/collidine. Consistent with this finding, the time-dependent spectral changes that follow excitation of **[PZn−PFe-(collidine)]**$^+$ in these two solvent systems are similar, indicating that, at least for polar aprotic solvents, modulation of solvent dielectric does not substantially influence the observed electron-transfer dynamics. Transient absorption spectra recorded at time delays longer than 20 ns (Supporting Information, Figure S9) rule out the presence of a long-lived excited-state having a high spin multiplicity as a contributing factor to the excited-state relaxation dynamics exhibited by this species.

The dynamics and transient absorption spectral features exhibited by electronically excited [**PZn−PFe-(collidine)]**$^+$ in 10:1 toluene/collidine (Figure 8b), interestingly, resemble those established for **PZn−PFe-Cl** (Figure 6), **[PZn−PFe-(py)$_2$]**$^+$, and **[PZn−PFe-(4-CN-py)$_2$]**$^+$ (Supporting Information) in polar solvents. Like the time-dependent transient absorption spectral features exhibited by electronically excited **PZn−PFe-Cl** in the methylene chloride solution (Figure 6), no cation radical spectral signature is manifest in the **[PZn−PFe-(collidine)]**$^+$ excited-state dynamics recorded in 10:1 toluene/collidine; all the observed dynamical processes contribute to fast or ultrafast recovery of the ground electronic state. Also noteworthy is the fact that while the ground-state electronic absorption spectrum of [**PZn−PFe-(collidine)]**$^+$ differs substantially from that determined for **PZn−PFe-Cl**, **[PZn−PFe-(py)$_2$]**$^+$, and **[PZn−PFe-(4-CN-py)$_2$]**$^+$ in methylene chloride solvent, the electronic absorption spectra of **PZn−PFe-Cl** in methylene chloride solvent and **[PZn−PFe-(collidine)]**$^+$ in 10:1 toluene/collidine solution are nearly identical (Supporting Information, Figure S8). This observation is thus consistent with the finding that transient dynamics evident for **[PZn−PFe-(collidine)]**$^+$ in 10:1 toluene/collidine solution (Figure 8B) resemble those manifested by **PZn−PFe-Cl** in CH_2Cl_2 (Figure 6).

The fact that increasing the solvent polarity from methylene chloride to benzonitrile results in almost no change in the **[PZn−PFe-(collidine)]**$^{+*}$ electron−transfer dynamics, while use of toluene solvent completely suppresses photoinduced charge separation, can be rationalized from solvent-dependent NMR spectroscopic data. The NMR spectrum of **PFe(III)** in 10:1 CD_2Cl_2/collidine manifests two aromatic collidine resonances [$\delta \approx$ 6.8 ppm (free collidine) and $\delta \approx$ 8.0 ppm (ligated collidine)], whereas similar spectra recorded in 10:1 toluene-d_8/collidine manifest only one collidine signal [$\delta \approx$ 6.46 ppm]. These data indicate that dissolution in toluene inhibits collidine binding, even when this ligand is present at a several 1000-fold molar excess. This result likely derives from inadequate solvation of free chloride ions in a nonpolar medium.[135]

Excited-State Dynamics of [PFe-(L)$_{1,2}$]$^+$ **Species.** To provide added insight into the origin of the unique excited-state dynamics manifested by electronically excited [**PZn−PFe-(collidine)]**$^+$ in polar solvents with respect to that evident for **PZn−PFe-Cl**, **[PZn−PFe-(py)$_2$]**$^+$, and **[PZn−PFe-(4-CN-py)$_2$]**$^+$, comparative excited-state dynamical studies were carried out for **[PFe-(collidine)]**$^+$, **PFe-Cl**, **[PFe-(py)$_2$]**$^+$, and **[PFe-(4-CN-py)$_2$]**$^+$. Figure 9 contrasts the excited-state decay dynamics of **[PFe-(collidine)]**$^+$and **PFe-Cl** in dichloromethane solvent. For **PFe-Cl**, the initially prepared electronically excited-state decays with a time constant $\tau_{avg} \approx$ 750 fs, consistent with previously delineated heme photophysics.[128,129] Identical to the trends observed in the excited-state dynamics of the **[PZn−PFe-(L)$_{1,2}$]**$^+$ complexes (vide supra), ligation of pyridine and 4-cyanopyridine results in no change of the transient spectral signature and observed decay dynamics characteristic of **PFe-Cl** (data not shown). On the other hand, **[PFe-(collidine)]**$^+$ displays unique excited-state dynamics: following photoexcitation, this compound exhibits a fast relaxation component ($\tau \approx$ 1 ps, $A \approx$ 72%), as well as longer characteristic relaxation times of ~7 ps ($A \approx$ 18%) and 655 ps ($A \approx$ 10%); such long-lived ferric porphyrin excited-states are without precedent. Additionally, **[PFe-(collidine)]**$^+$ excited-state dynamics follow the same solvent-dependent trends established for **[PZn−PFe-(collidine)]**$^+$: nonradiative lifetimes determined for [**PFe-(collidine)]**$^+$ in toluene are consistent with data indicating that collidine is incapable of displacing **Cl**$^-$ from **PFe-Cl** in nonpolar solvents.

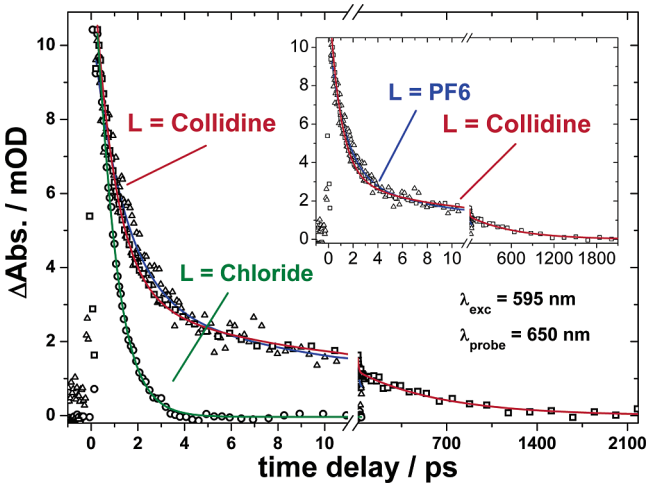

Figure 9. Excited-state decay profiles probed at 650 nm for **PFe-Cl** (○) in methylene chloride solvent and **[PFe-(collidine)]**$^+$ (□) in 10:1 methylene chloride/collidine; λ_{ex} = 595 nm. The solid lines were determined from multiexponential fits of the transient data. (Inset) Excited-state decay profiles under identical conditions for **[PFe-(collidine)]**$^+$ (□) in 10:1 methylene chloride/collidine and **PFe-PF$_6$** (△) in methylene chloride solvent.

Scheme 2 summarizes the excited-state relaxation dynamics of **[PZn−PFe-(L)$_{1,2}$]**$^+$. Excited-state deactivation of **[PZn−PFe]** is both solvent and **PFe**$^+$ ligation-(spin)-state dependent; these factors determine the relative magnitudes of charge separation (k_{cs}) and nonradiative(k_{nr}) rate constants. The driving force for charge-separation, ΔG_{cs}, can be estimated from the Weller equation:[136]

$$\Delta G_{cs} = e[E(\mathrm{ox})_D - E(\mathrm{red})_A] - E_{0,0} - \frac{e^2}{4\pi\epsilon_o\epsilon_s}\left(\frac{1}{R_{DA}} - \frac{1}{2R_D} - \frac{1}{2R_A}\right) \quad (8)$$

where $E(\mathrm{ox})_D$ and $E(\mathrm{red})_A$ are the oxidation and reduction

(135) The similarity of electron-transfer dynamics between the methylene chloride and benzonitrile experiments is not as simple to rationalize. This result may derive in part from a local solvation environment dominated by collidine, or from the large driving force for charge separation (~−1.3 eV).

Scheme 2. Energy Level Diagram Showing the Major Decay Pathways of $[PZn-PFe\text{-}(L)_{1,2}]^+$ Excited States

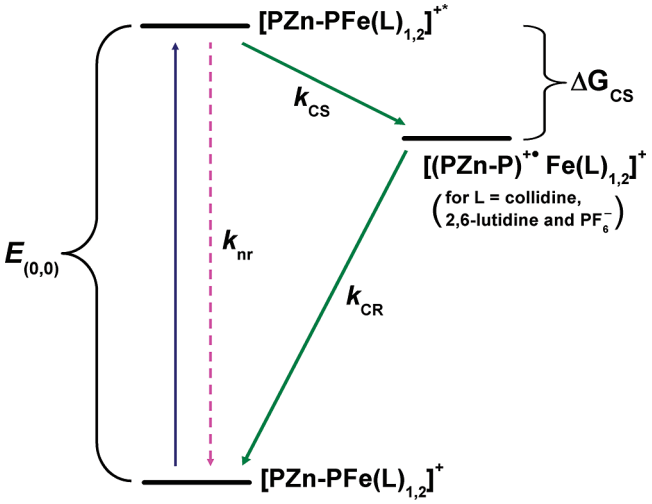

potentials of the porphyrin and iron center, respectively. The D (R_D) and A (R_A) reactant sizes and the center-to-center distance (R_{DA}) determined from ZINDO optimized structures are $R_D = R_A \approx 5.7$ Å and $R_{DA} \approx 11.9$ Å. Using these parameters and the potentiometric data reported in Table 1 highlights that ΔG_{cs} for **[PZn−PFe-(L)$_{1,2}$]$^+$*** is strongly influenced by the PFe^+ ligation state [ligand (ΔG_{CS}): 4-cyanopyridine (−0.79 eV) < pyridine (−1.04 eV) < collidine (−1.35 eV) < chloride (−1.40 eV); solvent = CH_2Cl_2]. Note that the pump−probe transient absorption dynamics elucidated for **[PZn−PFe-(L)$_{1,2}$]$^+$** species are not correlated with the thermodynamic driving force for photoinduced charge separation, as the $[(PZn-P)^{+\bullet}\ Fe^{II}(L)]^+$ transient signal was only observed following optical excitation of **[PZn−PFe-(collidine)]$^+$**.

For **PFe(II)** and **PFe(III)** complexes, it has been established previously that k_{nr} is fast [$>(1 \times 10^{-12})$ s^{-1}].[128,129] It would thus be expected that strongly conjugated **[PZn−PFe-(L)$_{1,2}$]$^+$** supermolecules would possess low quantum yields for charge separation regardless of the **PFe$^+$** ligation state, due to the prominent role played by the Fe open *d* shell in facilitating fast excited-to-ground-state internal conversion. Collidine (and 2,6-lutidine, not shown) coordination to **[PFe]$^+$** followed by optical excitation clearly causes a significant fraction of **[PFe]$^+$*** states to decay via a nonradiative process that is unusually slow with respect to all other $[PFe\text{-}(ligand)_{1,2}]^+$ systems studied to date (Figure 9). The origins of this effect remain unclear, but differences in spin state, iron oxidation potential, and a chloride-derived heavy-atom effect can be eliminated as possible explanations by the above-described experiments. In contrast to the other ligands studied, collidine's 2- and 6-methyl groups give rise to significant steric interactions with the macrocycle plane. Such steric parameters are known to significantly distort the planarity of the ferric porphyrin macrocycle[107] and also to contribute to ferric ion doming.[106,107,137] To assess whether ferric-ion doming and weak metal axial ligand interactions may be partly responsible for the unique excited-state decay dynamics of **[PFe-(collidine)]$^+$**, **[PFe]$^+$[PF$_6$]$^-$** was prepared by ligand metathesis from **PFe-Cl**. Remarkably, the excited-state decay dynamics of **[PFe]$^+$[PF$_6$]$^-$*** are almost exactly superimposable with those delineated to **[PFe-(collidine)]$^+$** (Figure 9, inset), suggesting that the combination of doming and a weak **Fe^{III}** axial ligand interaction may commonly give rise to $[PFe\text{-}(ligand)_1]^+$ complexes with unusually long excited-state lifetimes. Whether the genesis of this effect is due to a reduction in the degree of overlap between the partly filled iron *d*-orbitals and porphyrin π-symmetric molecular orbitals beyond some critical amount, or to more obscure factors such as an altered landscape of accessible excited-state nuclear relaxation modes, is not presently known.

Whatever the origin of this effect, it is clear that the significant reduction in the magnitude of k_{nr} observed for **[PFe-(collidine)]$^+$*** (and for **[PFe-(2,6-lutidine)]$^+$***, **[PFe]$^+$*[PF$_6$]$^-$***) relative to that evinced for all other electronically excited **[PFe-(ligand)$_{1,2}$]$^+$** complexes plays an important role in determining the observed **[PZn−PFe-(collidine)]$^+$*** dynamics. Once k_{nr} is significantly diminished, charge separation becomes a competitive excited-state deactivation pathway in **[PZn−PFe-(collidine)]$^+$***. Thus, despite the fact that ΔG_{CS} (4-cyanopyridine) > ΔG_{CS} (pyridine) > ΔG_{CS} (collidine) > ΔG_{CS} (chloride), the collidine-ligated species exhibits photoinduced charge separation due to the apparent inability of the iron open *d* shell to provide an efficient pathway for fast, nonradiative decay.

Conclusion

We have synthesized and examined the spectroscopy, potentiometric properties, and transient dynamics of strongly coupled *meso*-to-*meso* ethyne-bridged bis[(porphinato)metal] complexes that possess Zn(II) and Fe(III) centers in a variety of axial ligand (L) environments [pyridine (py), 4-cyanopyridine (4-CN-py), 2,6-dimethylpyridine (2,6-lutidine), and 2,4,6-trimethylpyridine (collidine)]. The excited-state transient dynamics of **[PZn−PFe-(L)$_{1,2}$]$^+$** supermolecules as well as several [(porphinato)iron−$(ligand)_{1,2}]^+$ (**[PFe-(L)$_{1,2}$]$^+$**) benchmarks were interrogated using pump−probe spectroscopy. Femtosecond time scale transient absorption spectroscopic experiments show that monomeric **[PFe(L)$_{1,2}$]$^+$** complexes **PFe-Cl**, **[PFe-(py)$_2$]$^+$**, and **[PFe-(4-CN-py)$_2$]$^+$** demonstrate subpicosecond-to-picosecond relaxation dynamics; the observed ultrafast ground-state recovery is consistent with the expectation that the partially occupied heme *d*-manifold provides a multiplicity of states that facilitate large-magnitude nonradiative decay rate constants.[127−129] Interestingly, the electronically excited states of **[PFe-(collidine)]$^+$**, **[PFe-(2,6-lutidine)]$^+$**, and **[PFe]$^+$[PF$_6$]$^-$** all manifest dynamics that feature a significant, slow ground-state recovery component with a time constant in excess of 0.5 ns; such long-lived (porphinato)-iron(III) electronically excited states have heretofore been without precedent.

Comparative pump−probe transient absorption experiments that interrogate the initially prepared excited states of **PZn−PFe-Cl**, **[PZn−PFe-(py)$_2$]$^+$**, **[PZn−PFe-(4-CN-py)$_2$]$^+$**, **[PZn−PFe-(collidine)]$^+$**, and **[PZn−PFe-(2,6-lutidine)]$^+$** demonstrate that the spectra of all these species are dominated by a broad, intense NIR $S_1 \rightarrow S_n$ transient absorption manifold. This absorptive feature is a spectroscopic hallmark of this class of highly conjugated multichromophoric compounds:[62,125,126] such signals are absent from transient absorption spectra recorded for monomeric porphyrinoid species and from less-strongly coupled multiporphyrin ensembles.[62] While **PZn−PFe-Cl***, **[PZn−PFe-(py)$_2$]$^+$***, and **[PZn−PFe-(4-CN-py)$_2$]$^+$*** evince

(136) Weller, A. *Z. Phys. Chem. N. F.* **1982**, *133*, 93−98.
(137) Scheidt, W. R. *Acc. Chem. Res.* **1977**, *10*, 339−345.

subpicosecond and picosecond time-scale relaxation of their respective initially prepared electronically excited states to the ground state, the excited-state dynamics observed for **[PZn−PFe-(2,6-lutidine)]**$^{+}$* and **[PZn−PFe-(collidine)]**$^{+}$* show fast relaxation to a [PZn^{+}−PFe(II)] charge-separated state having a lifetime of nearly 1 ns. Potentiometric data indicate that while ΔG_{CS} for **[PZn−PFe-(L)$_{1,2}$]**$^{+}$* species is strongly influenced by the PFe^{+} ligation state [ligand (ΔG_{CS}): 4-cyanopyridine (−0.79 eV) < pyridine (−1.04 eV) < collidine (−1.35 eV) < chloride (−1.40 eV); solvent = CH_2Cl_2], the pump−probe transient absorption dynamical data demonstrate that the nature of the dominant excited-state decay pathway is not correlated with the thermodynamic driving force for photoinduced charge separation but depends on the ferric ion ligation mode. Sterically bulky axial ligands (that drive a pentacoordinate PFe center and a weak metal axial ligand interaction) serve to sufficiently suppress the normally large-magnitude, nonradiative decay rate constants characteristic of (porphinato)iron(III) complexes, and thus make electron transfer a competitive excited-state deactivation pathway for **[PZn−PFe-(L)$_1$]**$^{+}$ supermolecules. While ascertaining the genesis of these effects will require further study, the data reported herein suggest that the combination of metal doming and a weak **Fe^{III}** axial ligand interaction may commonly give rise to pentacoordinate **[PFe-L$_1$]**$^{+}$ complexes with uncharacteristically long excited-state lifetimes. Such ligand environments for (porphinato)iron(III) centers will enable fabrication of PFe(III)-based strongly coupled multipigment materials and supramolecular ensembles in which charge-transfer dynamics play an unusually prominent role.

Acknowledgment. This work was supported by the National Institutes of Health. T.V.D. thanks the Department of Education for a GAANN pre-doctoral fellowship. M.J.T. is indebted to the Office of Naval Research and the MRSEC Program of the National Science Foundation for equipment grants for transient optical instrumentation. We are grateful to Dr. H. C. Fry for the preparation of the [**PFe**]$^{+}$[**PF$_6$**]$^{-}$ complex.

Supporting Information Available: Transient spectral data and decay-associated spectra for electronically excited **[PZn−PFe(L)$_{1,2}$]**$^{+}$ and **[PFe(L)$_{1,2}$]**$^{+}$ species. This material is available free of charge via the Internet at http://pubs.acs.org.

JA061388M